THESIS

METALS EXPORT TO STREAMS DURING BASE FLOW AND STORM EVENTS IN THE 416 FIRE, SOUTHWEST COLORADO

Submitted By

Bryce A. Pulver

Department of Ecosystem Science and Sustainability

In partial fulfillment of the requirements

For the Degree of Master of Science

Colorado State University

Fort Collins, Colorado

Spring 2021

Master's Committee:

Advisor: Stephanie K. Kampf

Matthew R.V. Ross

Stephen J. Leisz

ABSTRACT

METALS EXPORT TO STREAMS DURING BASE FLOW AND STORM EVENTS IN THE 416 FIRE, SOUTHWEST COLORADO

With approximately two thirds of the Western U.S. relying on fresh water from forested areas, it is vital to understand how wildfires can affect the release of metals into soil water and streams. Moderate to high intensity fires can alter the physical and chemical properties of soil, allowing elevated release of sediment, organic matter, and nutrients to streams. While many studies have focused on how fires affect sediment loading, nutrient export, and organic matter; less research has been conducted on how wildfire impacts the export of metals. This study examines metals export from the 2018 416 fire near Durango, CO during baseflow and storm events. Six tributaries (3.88-38.8 km^2) and five sites on Hermosa Creek (152-435 km^2) were sampled and analyzed for metal concentrations. We examine how metal concentrations relate to burn severity and watershed characteristics under different flow conditions using both univariate correlation analysis and multivariate models. Metal concentrations were significantly greater in burned baseflow samples compared to unburned locations for As, Ca, K, Mg, Mo, Si, Sr, and Zn. Concentrations of As in baseflow exceeded the Environmental Protection Agency's (EPA's) primary drinking water maximum contaminant level (MCL). Metal concentrations in baseflow were positively correlated with percentage of watershed burned, burn severity, and basin slope, and negatively correlated with basin elevation, drainage area, and average annual precipitation. Metal concentrations increased significantly (mean factor change = 20.6) in storm samples compared to pre-storm samples for Al, As, Ba, Ca, Cr, Fe, K, Li, Mg, Mn, Si, and Zn with Al,

As, Ba, Be, Cd, Cr, Fe, Mn, Ni, and Pb being above an EPA or World Health Organization (WHO) MCL. Although storm samples were limited, metal concentrations were correlated with watershed burn severity ($r \sim 0.8$), indicating elevated metal concentrations likely came from burned areas. Overall, this study demonstrated that wildfires cause elevated metal concentrations in both baseflow and stormflow, but with the exception of As, only the stormflow metal concentrations posed water quality concerns, with 10 metals exceeding both EPA and WHO MCL's for drinking water.

ACKNOWLEDGEMENTS

I would like to thank all the wonderful people who helped in this research project. Stephanie Kampf, who has been such a kind and knowledgeable advisor. She has been instrumental to my growth as a scientist, by navigating through various research topics, being patient with learning a new field of study, and showing me what it means to be a graceful academic and leader. Matt Ross, who has opened my eyes to the wonderful world of coding and is an encyclopedia of enthusiasm and biogeochemical knowledge. Steve Leisz, who re-sparked my fascination with space and showing me how remote sensing applications are virtually limitless. My appreciation goes out to Charles Rhoades and Tim Fegal for allowing me to brainstorm on chemistry related topics and use their instrumentation resources at the Rocky Mountain Research Station. Heidi Steltzer and Gigi Richard at Fort Lewis College for them allowing me to have a home base of logistics and provide field guidance. Scott Roberts for being my direct contact to the community through his involvement with the Mountain Studies Institute and US Forest Service and coming out into the field.

A special thank you goes out to my research group and graduate student offices mates for playing a role of constant support and scientific discussion. My research would not be where it is today without the insights and conversations with Alex Brooks, Allie Rhea, Karin Emanuelson, Eric Jensen, Abby Eurich and Katie Willi. My deep appreciation goes to The American Indian Graduate Fund, The Office of Navajo Nation Scholarship & Financial Assistance, the PRSE CSU Fellowship, The Hill Memorial Fellowship, and The Colorado Mountain Club for funding my research.

I would also like to thank all my family and friends for supporting me through this wild ride. My Parents for their constant unwavering willingness to help and support this endeavor. My Brother who always offered me relief from the daily routine and has inspired me for as long as I can remember. And I would like to acknowledge all of the ancestral lands of the Diné Bikéyah, Ute, Pueblo, and Apache nations were I conducted my research.

There were so many wonderful lessons learned on this journey, thank you all.

DEDICATION

In loving memory of my Grandmother, Stella Largo. You were the kindest, strongest, and most loving woman that has ever been a part of my life.

Ayóó ánítíníshí, ahéhee'. Nizhónígo ch'aanidíínaał.

TABLE OF CONTENTS

1. INTRODUCTION

Wildfires in North American forests have increased greatly in area, duration, frequency, and severity since the mid-1980s due to higher spring and summer temperatures, changes in land use and management, and reduced winter precipitation. (Jolly et al. 2015; Miller et al. 2009; Westerling et al. 2006; Williams et al. 2010). In the Western United States, mountain forests have seen the largest increase of these effects; while these forests account for approximately one third of land cover, around 65% of fresh water originates from forested land (Brown, Hobbins, and Ramirez 2008; Miller et al. 2009; USDA Forest Service 2014; Westerling et al. 2006). With an average of 6.6 million acres burned each year over the past 10 years it is paramount to understand how these fires may impact watershed health (Hoover 2018).

Following wildfires, soil infiltration capacity declines, and overland flow increases, leading to increased erosion rates (Debano 1990; Heydari et al. 2017; Kampf et al. 2016a; Ryan, Dwire, and Dixon 2011). Changes in runoff and erosion after fire increase fluxes of sediment, nutrients, trace elements, and organic matter into watersheds, potentially to detrimental and toxic levels (Abraham, 2017). Prior studies have found that first year post-fire exports of sediment, total N, total P, NO_3^-/ NO_2^-, and NH_3/NH_4^+ to watersheds all increase, and the elevated export may persist for up to 10 years after fire (Smith et al. 2011). While multiple studies have examined nutrient export after fires (Kong, Yang, and Bai 2018; Rust et al. 2019), limited research has examined the export of trace metals in a post-fire environment. The few studies that have been conducted have found values exceeding the limits of the World Health Organization (WHO) guidelines (WHO 2017) for Fe, Mn, As, Cr, Al, Ba, and Pb, while Cu, Hg, and Zn have had post-fire concentrations at the limits or just above WHO guidelines (Gallaher et al., 2003;

Townsend et al. 2004; White et al. 2006, Murphy 2020).

In forest catchments, the amount of metals in soils is related to soil organic matter (SOM), clay properties, and microbial communities (Reis et al. 2015). Once introduced to forest catchments through weathering, metals can accumulate in organic layers of the soil, sediment, complexed SOM, and plants (Biester et al. 2002; Kabata-Pendias 2012; Shcherbov 2012). These biogeochemical components are generally responsible for keeping major and trace metals relatively insoluble resulting in low mobilization of metals in the soil profile. As such, metals concentrations tend to decrease rapidly with soil depth (Ruan et al. 2008). During fire, plant biomass and litter are consumed, generating temperatures high enough to alter the physical and biogeochemical properties of soil, potentially releasing some of these metals from their immobile complexations. The exact release mechanism of any metals post-fire depends on pre-fire soil concentrations, soil type, vegetation density and type, fire severity, maximum temperature reached during the fire, and fire dynamics (Certini 2005; Pereira, Úbeda, and Martin 2012; Someshwar 1996). Previous studies have established that fire is able to release and remobilize sequestered metals from plants and SOM, and these released metals can move into soils or the atmosphere (Biswas et al. 2007). Fire also decreases organic matter and clay in soils while increasing pH, which will also increase metal mobilization (Norouzi and Ramezanpour 2013), because there are fewer binding sites to hold the metals in soil. These chemical processes can also influence physical characteristics of soils, such as stability, aggregation, and pore space, which can lead to physical erosion rates 2-100 times above pre-fire rates (Abraham et al. 2017; Debano 1990).

While the limited set of studies on post-fire metals release to streams indicate a potential problem, none have yet explored the hydrologic controls on metals export. The objective of this

study is to explore how watershed characteristics and burn variables interact with hydrologic condition (storm or baseflow) to control trace metal concentrations in streams.

2. SITE DESCRIPTION

The study area is the 416-fire, which burned 223 km^2 in southwestern Colorado in June-July 2018 (Figure 1). Most of the burned area is part of the Hermosa Creek drainage basin, approximatively eight miles north of Durango, CO (Figure 1). The fire was started by embers from a coal-powered train, and it burned from June 1st – July 31st. The burn covered roughly 51% of Hermosa Creek's watershed (435 km^2) and had spatially variable severity with roughly 33% of the area having moderate or high soil burn severity (Hansen 2019). Hermosa Creek feeds into the Animas River, contributing ~10% of the Animas flow recorded at the stream gauge in Durango. The headwaters are along the border between Dolores and San Juan counties, fed by springs and streams that create a set of wetlands in the upper basin (2670-3840 m). The open upper basin transitions into a narrow valley, cutting through Permian rock between the Rico Mountains to the west and Graysill and Engineer Mountains to the east. Hermosa Creek (19.8 m/km) continues to cut though sedimentary formations of shales, siltstones, mudstone, limestone, and arkosic grit for about 30 km with many perennial and intermittent stream contributions. The river gradient becomes gentler next to the town of Hermosa, CO, before joining with the Animas River.

The basin is part of the San Juan mountain range, and the dramatic changes in elevation cause large variability in climate within the watershed. Climate stations located in Durango (2012 m) and Silverton (2826 m), CO (WRCC) report average annual total precipitation ranging from 532-622 mm and average snowfall from 1646-3965 mm. The average annual daily maximum temperature ranges from 17.4-11.2 °C and the average annual daily minimum temperature ranges from -7.6 to 0.9° C. Hermosa Creek has a snowmelt dominated hydrograph,

which is characterized by a large increase in flow during late spring, with brief increases in the summer due to monsoonal storms.

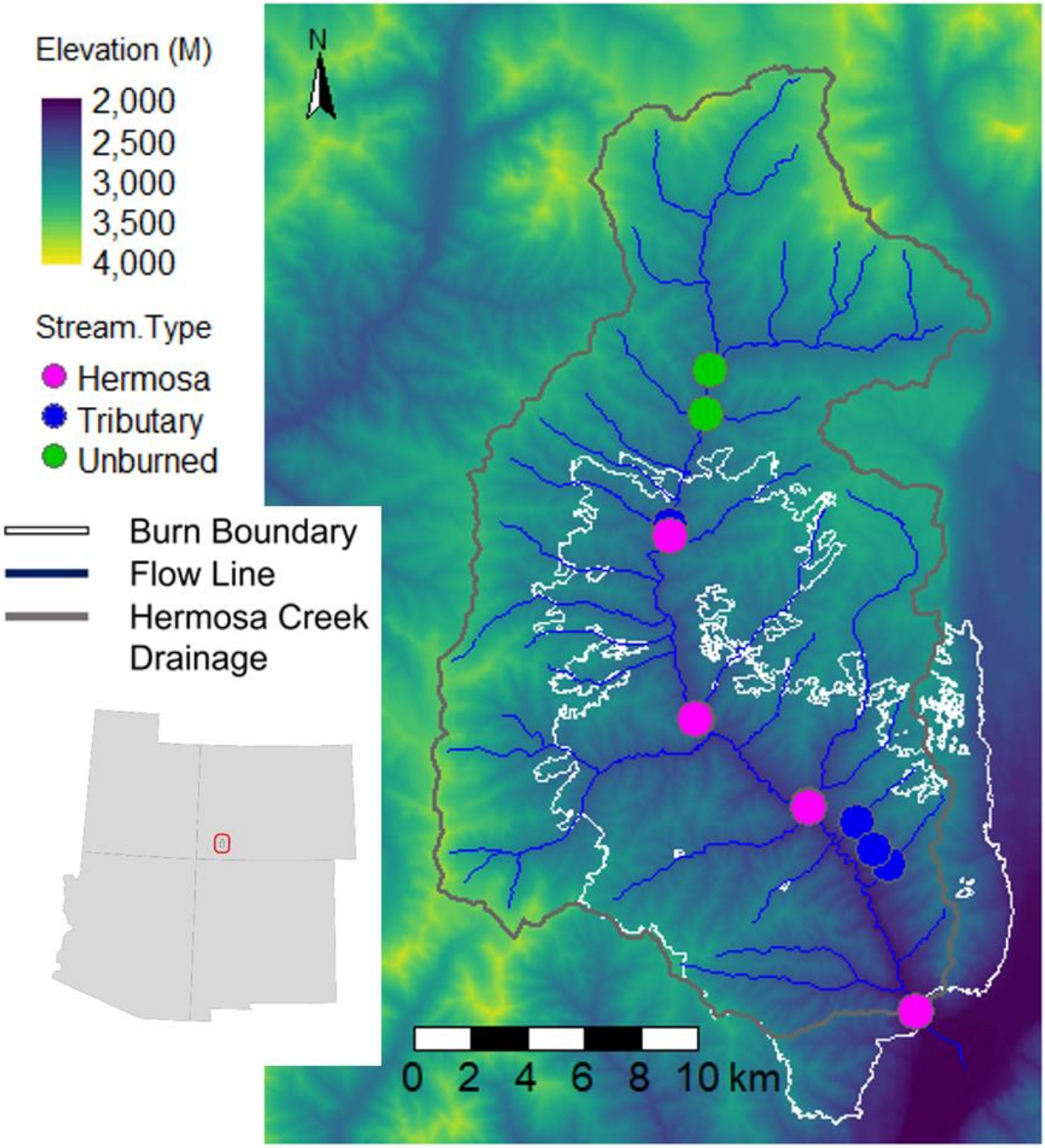

Figure 1: Map of Hermosa Creek watershed showing 416 fire boundary and sampling locations. The inset map is of the four corner states with the burned area highlighted in red. Base map is elevation.

The Pennsylvanian Molas formation is at lower elevations overlain by the Hermosa Formation and Rico Formation at mid to lower elevations (2050-3200 m) and the Permian Cutler Formation at upper elevations (>3200 m). The Cutler and Hermosa Formations are the thickest at about 600 m, whereas the Rico and Molas formations are <100 m in thickness (Eckel 1949; Gonzales 2004; Steven 1974). Soils in the watershed are a complex of deep and shallow well-drained soils derived from red bed sandstone and shale. They are mapped as Haviland-Needleton complex, 30 to 60 percent slopes; Graysill-Scotch complex, 30 to 60 percent slopes; and Hourglass-Wander complex, 5 to 30 percent slopes (USDA 2007). These soils have low to moderate erodibility (Hansen 2019).

Hermosa Creek has mainly undeveloped land, with <0.1% agricultural land cover. The land is managed by the National Forest Service and is designated free range for cattle. The watershed is dominated by montane and subalpine forest, covering low angle riparian zones into high angle slopes to the edge of the alpine tree line (~11,500 ft). Vegetation in the riparian corridor is dominated by blue spruce (*Picea pungens*) with thinleaf alder (*Alnus incana*), Drummond's willow (*Salix drummondiana*), and Rocky Mountain willow *(Salix monticola*). Other common species in the riparian zone include elderberry (*Sambucus cemose*), meadowrue (*Thalictrum fendleri*), chokecherry (*Prunus virginiana*) and Richardson's geranium (*Geranium richardsonii*). The drier slopes are dominated by Engelmann spruce (*Picea engelmannii*) (Lyon et al. 2003).

3. METHODS

3.1.Field/Lab Methods

Within the 416 fire, 11 stream sampling sites were selected to capture a range of drainage areas (0.1 – 435 km^2) and burn severity (Figure 2). The sample locations include six tributary, three main drainage, and two control (unburned) sites. The sampled sites were all steep (35-53%), varied in burn percentage (6-99%), and watershed average burn severity ranged from low to moderate according to dNBR (0.17-0.47) (Table 1). At each site, water samples were collected during summer monsoon storm events and during base flow, starting at the beginning of June to November. A total of 41 sample sets were collected, of which most were base flow. Due to hard to predict isolated thunderstorms, only two sets of storm samples were collected at three tributaries (T1-T4) before and after each storm event. The sampling schedule was roughly every two weeks and was conducted over a two-day period in the upper and lower basin of Hermosa Creek. The basin was too large to collect all samples in one day.

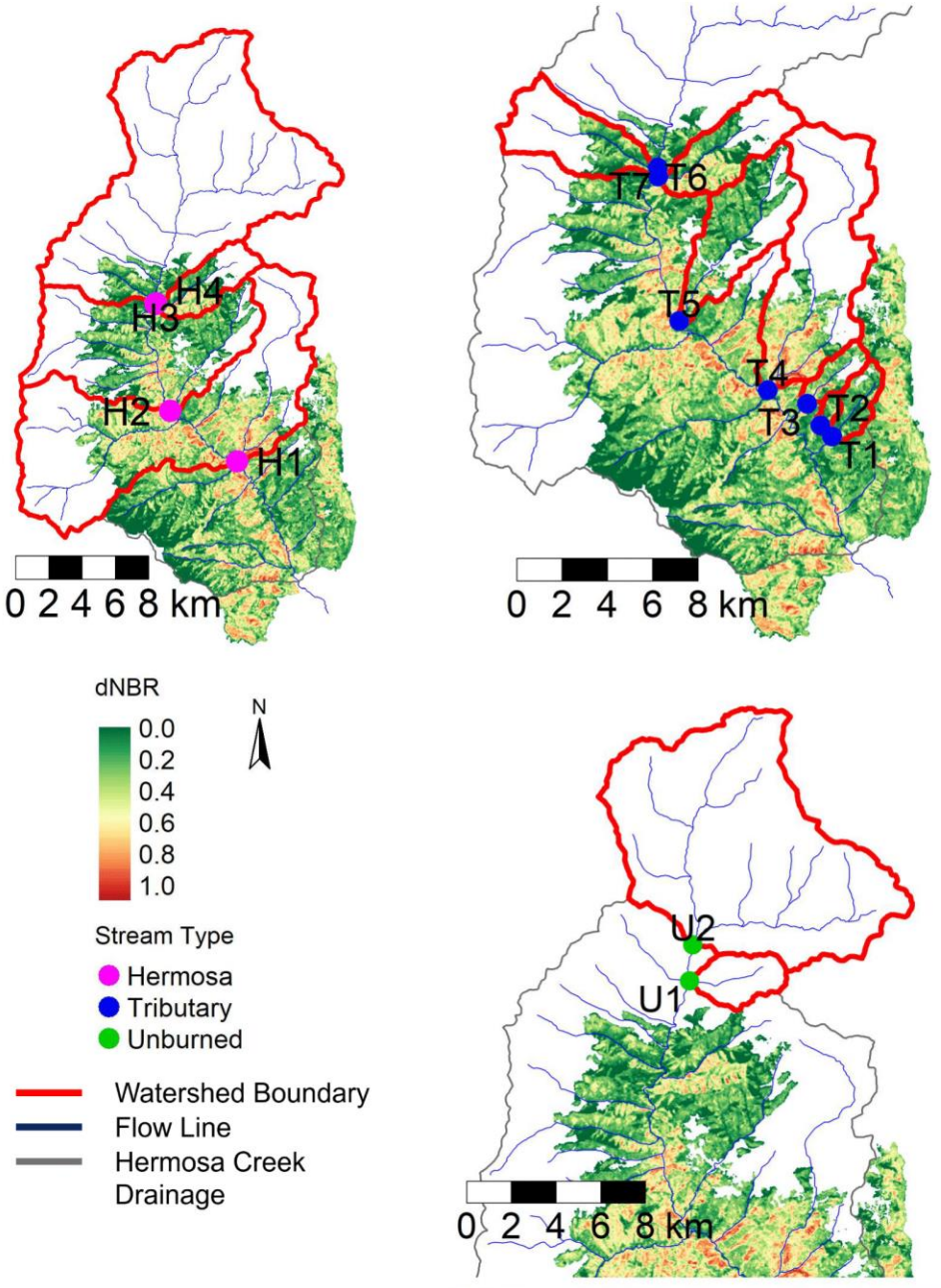

Figure 2: Site map showing the names of sampling sites and outlines of each watershed (red lines). dNBR is the normalized burn severity, with green showing low burn severity and red showing high severity. Pre-fire Landsat image was taken 05/17/18 and post-fire Landsat image was taken 11/09/18. Note: site ID numbers increase from the outlet of the basin to the headwaters.

Table 1: Watershed Characteristics for stream monitoring locations. Note: numbering is in order from lowest to highest part of the Hermosa drainage. The lettering abbreviation is as follows; T = tributary, H = Hermosa, and U = unburned. * This is elevation change along the longest flow path of the watershed

Site ID	Basin Slope (%)	Elev. Change*(m/km)	Drainage Area (km^2)	Mean Basin Elev. (m)	Average Burn Severity (dNBR)	% of Watershed Burned
T1	44	63	20	2903	0.21	94
T2	53	20	435	2923	0.22	99
T3	41	23	355	2983	0.31	78
T4	38	55	39	2940	0.47	30
T5	47	92	7	2979	0.21	62
T7	47	70	16	2965	0.18	34
T6	47	64	14	2964	0.31	60
H0	46	24	237	3010	0.30	43
H1	45	32	166	3059	0.33	30
H2	43	32	152	3067	0.25	25
H3	41	55	95	3139	0.23	11
H4	40	128	5	2781	0.17	6
U1	48	284	1	2646	NA	NA
U2	35	117	4	2827	NA	NA

Samples were collected using acid washed Nalgene bottles, consisting of a 50 mL filtered and unfiltered sample for metals analysis and a 250 mL sample for more general water quality analysis. Filtration was conducted in the field with a 0.45 µm nylon filter to avoid metals contamination and represent the bioavailable metals. Samples were transported in a cooler under ice and then stored in a refrigerator (<5 °C). Each metals sample was preserved in the lab with metals grade nitric acid (2%) (EPA method 200.8).

Pre- and post-storm samples with high turbidity and ash content were digested in a 1:1 solution of nitric acid using a hot block (85 °C) until 50% of the solution remained. Samples were left to cool, then brought back to the original volume with DI water. The digested sample represents the total recoverable analyte, and the preserved sample represents the bioavailable or

dissolved analyte. Samples were analyzed using Colorado School of Mines' ICP-AES (inductively coupled plasma-atomic emission spectroscopy) and the Rocky Mountain Research Station's IC (ion chromatography) for trace metals and major and minor ions. Concentrations of 28 metals (Al, As, B, Ba, Be, Ca, Cd, Co, Cu, Cr, Fe, K, Li, Mg, Mn, Mo, Na, Ni, Pb, Sb, Se, Si, Sn, Sr, Ti, Tl, V, Zn) were analyzed.

3.2. Watershed characteristics and burn severity

Ten variables, seven collected from USGS StreamStats (USGS 2016) and three from Landsat 8 images, were selected to evaluate watershed characteristics and burn severity. Watershed characteristics selected from StreamStats were average basin slope, change in elevation over the longest flow path, drainage area, mean basin elevation, and percent of watershed area covered by SSURGO soil type C and D. Basin slope is the average slope from all 10 m digital elevation grid cells in each watershed. Elevation change is calculated from the watershed's longest flow path with two points taken from 15 and 85% of the flow path length.

Burn severity indices from remote sensing data have been used in previous studies to assess how burn severity may affect the release of nutrients, more specifically N (Clarke, Knox, and Butler 2013; Kong et al. 2018; Koyama, Stephan, and Kavanagh 2012), and it may help identify burned catchments that may be prone to export metals during storm events through erosion and higher water solubility of metals. Difference normalized burn ratio (dNBR) was calculated using two scenes (05/17/18 and 11/09/18) from Landsat 8. More scenes would have been used, but cloud and snow cover percentage was too high over the burn area during the burn year. The November scene was deemed reliable since there was limited fall regrowth and still a defined burn outline. NBR was calculated using equation 1 for the pre and post fire scenes.

Equation 2 was used to calculate dNBR. All negative values were set to = 0, since anything below 0 would indicate increased vegetation growth or no burn.

$$NBR = \frac{(NIR - SWIR)}{(NIR + SWIR)} \quad \text{(eq. 1)}$$

$$dNBR = NBR_{prefire} - NBR_{postfire} \quad \text{(eq.2)}$$

For data analysis average burn severity was calculated using the differenced normalized burn ratio (dNBR) with two images from Landsat 8 and then averaged across each watershed. % of watershed burned was calculated from the burn area and drainage area for each watershed.

3.3.Data analysis

The full dataset includes filtered and unfiltered samples; burned and unburned sites, and baseflow and stormflow samples. I used ANOVA to evaluate whether there were significant differences in metal concentrations between each of these groups. Filtered and unfiltered samples were taken at the same time to determine whether metals were bound to larger particles or if they were dissolved. For baseflow models only filtered samples were used to represent the highest bioavailability of metals. For stormflow models only pre and post storm event samples were used, and these included a combination of filtered and unfiltered due to the high turbidity of samples, but the same digestion method was used on each sample to ensure the same amount of metals extraction. I also evaluated how the concentrations related to maximum contaminant levels (MCL) for WHO drinking water standards and EPA primary and secondary drinking water standards (Table 2A)

For those metals that had significant differences between burned and unburned sites, I conducted regression analysis to evaluate potential drivers of metals in stormflow and baseflow. I conducted only univariate correlation analysis for stormflow due to small sample sizes. For baseflow, I initially conducted a cross correlation analysis to isolate redundant variables. Then I applied multivariate regression models, for which the general formula is shown in equation 3, where y is equal to a metal concentration; β is the coefficient for a given variable, and x is the independent variable (Hothorn et al. 2008; Lenth 2020).

$$y = \beta_0 + \beta_1 x_1 + \beta_2 x_2 + \cdots + \beta_n x_n \quad \text{(eq. 3)}$$

Model selection was conducted by using a combination of backward stepwise selection and Akaike information criterion (AIC) (Barton 2020). First all variables are included, and the AIC for the full model is determined. One term is dropped and then a new AIC value is calculated; if the new AIC is lower the new model proceeds to have terms dropped one by one. This continues until dropping a term no longer lowers AIC. The focus of these models is to isolate effects that cause increased metals concentrations, so multicollinearity is of concern. After a model is determined the variance inflation factor (VIF) (Fox and Weisberg 2019) is calculated for each term. The term with the largest VIF is dropped until there are no terms that have a VIF value >4, indicating limited collinearity. Terms are then evaluated for statistical significance, and the term with the highest p-value is dropped until all terms are significant to produce a significant terms model. Both the reduced collinearity and significant terms model are evaluated for overfitting and to determine the relative contributions of each independent variable to the overall model using the standardized β coefficient term.

4. RESULTS

4.1.Baseflow

Metal concentrations in baseflow ranged from below detection limits up to concentrations in excess of MCL's. Of the 28 metals analyzed 18 had concentrations above the ICP-AES's detection limits (Table 2). Of these 18 metals, differences between burned and unburned sites ranged from -37% to 1115%. One metal, As, was above the MCL for EPA primary drinking water standard (0.01 ppm) for both unburned and burned samples (Figure 3). Three metals, B, Ba, and V had negative percent differences, indicating lower concentrations in burned sites relative to unburned, but only one of these declines was statistically significant (Ba). Nine metals (As, Ba, Ca, K, Mg, Mo, Si, Sr, Zn) had significant increases in concentrations at burned sites relative to unburned sites for baseflow (Table 3, Figure 3). None of these metals had significant differences between filtered and unfiltered samples (Table 3), which indicates that they were not bound to suspended particles. Al, Fe, and Mn did have significant difference between filtered and unfiltered samples, with higher concentrations in the unfiltered samples, indicating that they were bound to suspended particles.

Table 2: Summary statistics for all filtered metals that were observed during baseflow. Bolded rows had a statistically significant difference in concentrations from unburned sites. Note: NAs in the percent change column are caused by the analyte not being detected at the unburned sites.

	Concentration (ppm)					
Metal	Mean	Median	Max	Min	n	Factor Change
Al	0.011	0.006	0.040	0.001	15	2.24
As	**0.016**	**0.015**	**0.034**	**0.009**	**26**	**1.46**
B	0.080	0.054	0.233	0.016	20	0.92
Ba	**0.114**	**0.104**	**0.255**	**0.017**	**37**	**0.63**
Ca	**113**	**76.5**	**385**	**33.4**	**37**	**2.62**
Co	1.51E-03	1.47E-03	2.07E-03	1.11E-03	22	1.02
Cr	9.92E-04	9.92E-04	1.29E-03	7.75E-04	13	NA
Fe	9.16E-03	4.54E-03	4.89E-02	1.88E-03	31	1.29
K	**1.32**	**1.32**	**2.45**	**0.558**	**37**	**1.93**
Li	0.011	0.008	0.020	0.005	20	NA
Mg	**19.0**	**17.8**	**45.5**	**4.28**	**37**	**3.00**
Mn	7.46E-03	5.60E-03	4.52E-02	3.76E-04	37	1.06
Mo	**3.48E-03**	**2.83E-03**	**7.12E-03**	**1.31E-03**	**32**	**2.11**
Na	4.38	3.83	7.49	2.08	37	1.57
Si	**3.42**	**3.27**	**5.17**	**2.63**	**37**	**1.20**
Sr	**2.81**	**1.56**	**12.9**	**0.205**	**37**	**12.2**
V	5.63E-04	5.19E-04	8.99E-04	3.86E-04	9	0.86
Zn	**0.010**	**0.009**	**0.015**	**0.006**	**37**	**1.20**

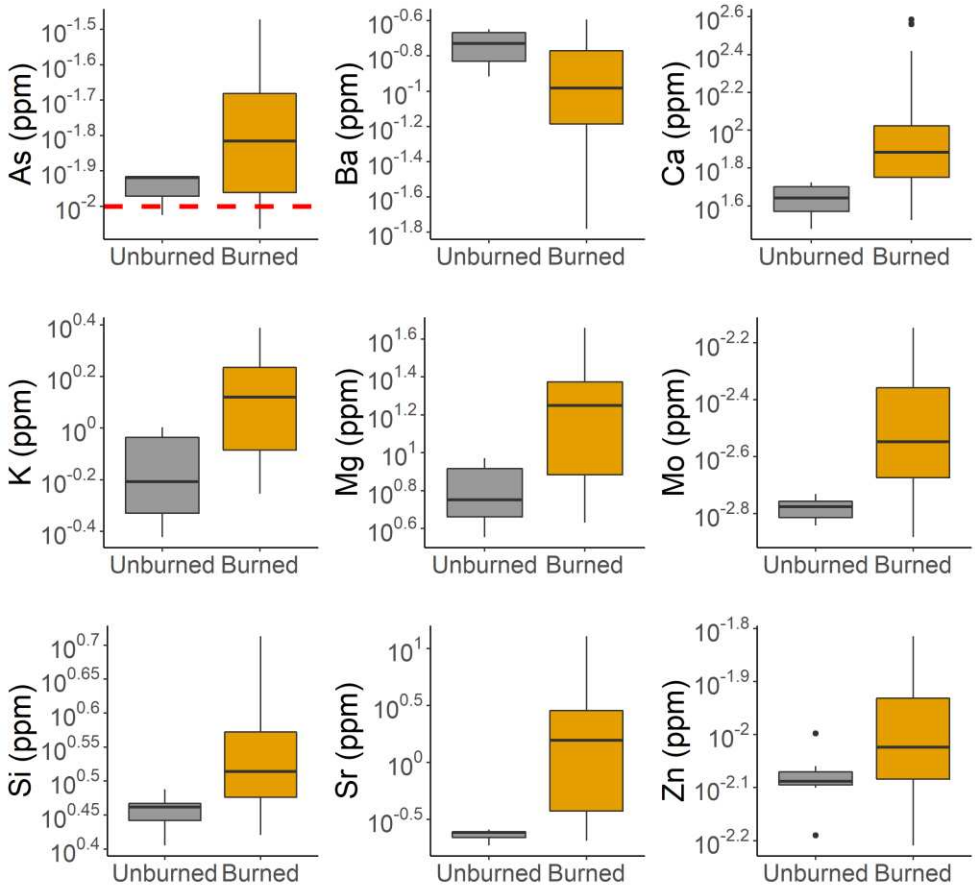

Figure 3: Concentrations of all metals with significant differences in concentrations between burned and unburned watersheds. Red dashed line is the MCL for EPA primary drinking water standard. Other MCL's are outside of the axis range shown.

Table 3: p-values for one-way ANOVA between filtered and unfiltered samples and between burned and unburned baseflow samples (n = 87). p-values for ANOVA on all (n = 22) pre-storm and post-storm flow samples. Bolded numbers are significant at p<0.05; red fill indicates increase; NA's indicate that insufficient data for comparison or not detected.

	p-value and direction of change					
Metal	Baseflow: Filtered vs Unfiltered	Unfiltered Conc.	Baseflow: Burned vs Unburned	Burned Conc.	Baseflow vs Stormflow	Stormflow Conc.
Al	**0.021**	↑*	**0.109**	↑	**0.049**	↑
As	0.604	↑	0.04	↑	**0.006**	↑
B	0.976	↓	0.954	↓	0.478	↑
Ba	0.88	↑	0.001	↓	**0.036**	↑
Be	NA		NA		0.266	↑
Ca	0.613	↑	0.006	↑	**0.048**	↑
Cd**	NA		NA		NA	
Co	NA		NA		0.079	↑
Cr	0.155	↑	NA		**0.032**	↑
Cu	NA		NA		0.068	↑
Fe	**<0.001**	↑*	**0.106**	↑	**0.032**	↑
K	0.882	↓	<0.001	↑	**0.01**	↑
Li	0.68	↓	NA		**0.006**	↑
Mg	0.564	↑	<0.001	↑	**0.007**	↑
Mn	**0.005**	↑*	**0.241**	↑	**0.039**	↑
Mo	0.78	↓	0.001	↑	0.986	↑
Na	NA		NA		0.246	↓
Ni	NA		NA		0.254	↑
Pb	NA		NA		0.238	↑
Si	0.055	↑	0.002	↑	**0.004**	↑
Sr	0.642	↑	0.003	↑	0.885	↑
Ti	NA		NA		0.447	↑
V	NA		NA		0.116	↑
Zn	0.281	↑	0.007	↑	**0.012**	↑

*Indicates arrows for unfiltered samples that were at least 2 times greater. All other unfiltered comparisons were close to 1:1.

**Cd was kept in table since it was detected in stormflow and above an MCL, but not detected any other time.

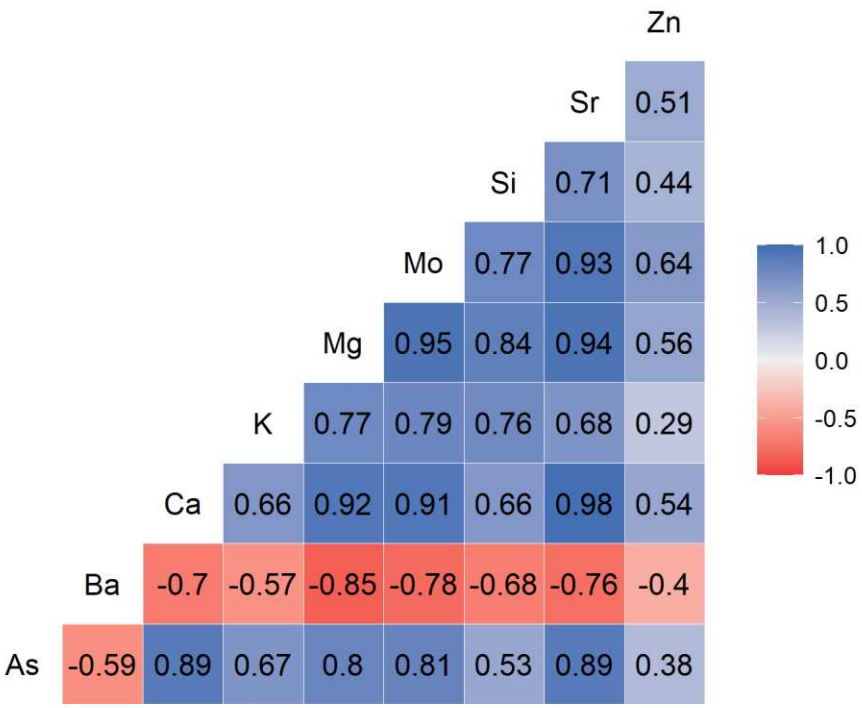

Figure 4: Correlation matrix for metals with significant differences in concentration (ppm) between burned and unburned sites for baseflow. Correlations are significant where Pearson correlation coefficients (r) are greater than 0.75.

The metals that had significantly different baseflow concentrations in burned and unburned watersheds exhibited high cross correlations in concentrations (Figure 4). Most metal concentrations were significantly correlated with each other ($\rho \geq 0.75$) except for Ba and Zn. Because many of the metal concentrations were so highly correlated, we focused our in-depth analysis on As, Ca, Si, Ba, and Zn. Ba (n = 37) concentrations are inversely correlated with all other metals (Figure 4). As (n = 26) has all observations exceeding the EPA limit of contamination (0.1 ppm). Ca has 37 observations, has the most normally distributed concentrations, and has lower correlations with the other selected metals. As and Ca are representative of K, Mg, Mo, and Sr not only due to their correlation with each other, but their

likelihood of complexation and ion exchange with subsurface minerals. Si was selected for not having a high correlation with Ca ($r = 0.66$) or As ($r = 0.53$) and also because of its abundance in the lithosphere and role in forming metal complexes (Al, Fe, heavy metals, and SOM) (Matichenkov and Bocharnikova 2001; Tubana, Babu, and Datnoff 2016) and Zn ($n = 37$) because it has the weakest correlation with any of the other metals.

We evaluated potential drivers of baseflow metal concentrations, by utilizing cross correlation analysis for the selected metals compared to watershed and burn characteristics. As and Ca (the representative metals for K, Mg, Mo, and Sr) are positively correlated with slope, change in elevation, and percentage of watershed burned; these metals are negatively correlated with mean annul precipitation and mean basin elevation (Figure 6, Appendix A). Si has a similar pattern of positive correlations with precipitation and mean elevation and negative correlations with change in elevation and percent burned, but only the correlation with percent burned area is significant. Zn has the same directions of correlations as As, Ca, and Si, but none of the relationships are significant. In contrast to the other example metals Ba is negatively correlated with change in elevation and percent burned but positively correlated with mean annual precipitation and mean elevation. Burn severity (μ dNBR or max dNBR) does not exhibit any significant correlation to metal concentrations at baseflow. As, Ca, and Zn, are positively correlated with soil type C and negatively related to soil type D. Conversely, Ba and Si have an indirect relationship with soil type C and a direct relationship with soil type D, the soil type with high runoff potential.

Figure 5: Correlation matrix between all watershed characteristics and burn variables vs baseflow filtered metal concentrations. Correlations are considered significant and bolded where Pearson correlation coefficients (r) are greater than 0.6.

Multivariate models illustrate the relative importance of the watershed and burn characteristics using the standardized β coefficients for each metal. Because the standardized coefficients are unitless, this allows comparing the strength of influence of the individual independent variables in the model. The highest standardized coefficient for six out of nine metals is percentage of watershed burned (Table 4); for two out of nine metals (Ca, Sr) the highest β values are for average annual precipitation, and for one metal (K) the highest β is for average basin elevation. Burn variables are more frequently included in the multivariate models than the other watershed characteristics, with each burn variable included in models for at least

five out of nine metals. Slope is also well represented in the models, included in six of nine models. Soil type (runoff potential classification) is also important for every metal expect Si.

The multivariate models had varying performance (Table 5). The highest performing multivariate model was for Mg, with an adjusted R^2 value of 0.93. Ba, Ca, K, Mo, Si, and Sr have all similar NRMSE and R^2 values (0.75 – 0.87). As and Zn both have low R^2 values (0.56 and 0.16) and higher NRMSE when compared to the rest of the response variable results. Using predicted R^2 as a metric to estimate how well each model will be at prediction, the two notable losses in performance are in the As and Zn model.

Table 4: Standardized coefficients for multiple regression models identified using backward stepwise selection and lowest AIC. Collinearity was considered for multivariate analysis, so all terms in the tables have VIF < 4. Bolded numbers are the numbers that have the highest absolute value of standardized β for each model. The bottom row (n) sums how many times each variable is included in a model.

Metal	Slope (%)	Drainage Area (km^2)	μ Elevation (m)	Precip. (mm)	SSURGO Type C Soil	SSURGO Type D Soil	% Watershed Burned	μ dNBR	max dNBR
As	0.307				0.312		**0.449**		
Ba	0.370	-0.240				0.499	**-1.172**		
Ca	0.436			**-0.671**		-0.398		0.354	-0.344
K			**-0.868**		-0.269			0.427	-0.319
Mg		0.474			0.472		**1.201**	0.429	-0.655
Mo		0.644			0.496		**1.260**	0.416	-0.815
Si	-0.422	0.283					**1.242**		-0.337
Sr	0.295			**-0.758**		-0.364		0.356	-0.310
Zn						-0.304	**0.437**		
n	5	4	1	2	4	4	6	5	6

Table 5: Performance statistics for each multivariate regression model. RMSE is normalized across the max and minimum value each metal to compare across response variables.

	As	Ba	Ca	K	Mg	Mo	Si	Sr	Zn
RMSE	0.004	0.027	34.2	0.241	3.30	5.90E-04	0.288	1.32	0.002
Y_{max} - Y_{min}	0.025	0.238	351	1.89	41.3	5.81E-03	2.53	12.6	0.009
NRMSE	0.17	0.11	0.10	0.13	0.80	0.10	0.11	0.10	0.23
Adjusted R^2	0.56	0.79	0.85	0.75	0.93	0.87	0.84	0.82	0.16
Predicted R^2	0.46	0.77	0.83	0.70	0.91	0.84	0.81	0.78	0.04
# of terms	3	4	5	4	5	5	4	5	2

4.2.Stormflow

Stormflow metal concentrations were analyzed for two monsoon season rainstorms on July 15th, 2019 and August 9th,2019. During both storms Hermosa Creek flash flooded, and turbidity levels rose above 1500 FNU at USGS gauge 09361500, downstream on the Animas River. Due to the size of the sampling region and timeframe of storms, samples were only collected at sites T1-T4 for a total of 22 samples. In these samples 26 of the 28 tested metals had concentrations above detection limits (Table 3). Of these, 12 metals (Al. As, Ba, Ca, Cr, Fe, K, Li, Mg, Mn, Si, Zn) had significant differences between pre and post storm flow (Table 3). 10 metals (Al, As, Ba, Be, Cd, Cr, Fe, Mn, Ni, and Pb) were above MCL's for post-storm samples and 4 metals (Al, As, Fe, and Mn) were above EPA primary and secondary MCL's for pre-storm samples.

Metal concentrations increased from 1.55-146x between pre- and post-storm samples (Table 6). There were more metals detected compared to baseflow, and they fell into three different groups. Group 1 metals are Al, As, Ba, Cr, Fe, and Mn. These metals had significant differences between pre-storm flow and post-storm flow concentrations and were above EPA and/or WHO contaminant limits. Group 2 metals are Be, Cd, Ni, and Pb. This group had concentrations that are above EPA and WHO contamination limits, but concentrations were not

significantly different between pre-storm and post-storm flow because the pre-storm samples had metal concentrations below detection levels, resulting in a low number of samples. Group 3 metals are Ca, K, Li, Mg Si, and Zn. These had significant difference between pre-storm flow and post-storm flow concentrations but did not exceed any contaminant limits. The rest of the metals detected (B, Co, Cu, Mo, Na, Sr, Ti, and V) did not have significant differences between pre-storm flow and post-storm flow concentrations, and they did not exceed any contaminant limits.

Table 6: Summary statistics of metal concentrations pre- and post-storm samples. Significant difference between pre- and post-storm samples at $p<0.05$. Concentrations above MCL labeled as Y (yes) if any sample exceeded at least one MCL.

		Concentration (ppm)					Sig. diff.	Concentrations> MCL
	Storm	Mean	Max	Min	n	Factor change		
Al	Post	30.2	96.6	0.039	8	18.9	Y	Y
	Pre	1.60	6.00	0.011	8			Y
As	Post	0.055	0.102	0.016	9	2.29	Y	Y
	Pre	0.024	0.044	0.010	12			Y
Ba	Post	1.42	5.60	0.025	9	23.7	Y	Y
	Pre	0.060	0.173	0.017	13			N
Cr	Post	0.023	0.070	0.001	9	7.67	Y	Y
	Pre	0.003	0.011	0.001	11			N
Fe	Post	29.7	132	0.002	9	24.6	Y	Y
	Pre	1.21	7.41	0.004	13			Y
Mn	Post	8.30	37.7	0.003	9	146	Y	Y
	Pre	0.057	0.406	0.001	13			Y
Be	Post	9.00E-03	2.10E-02	2.00E-03	4	30	N	Y
	Pre	3.00E-04	3.00E-04	2.00E-04	2			N
Cd	Post	0.008	0.015	0.003	3	NA	N	Y
	Pre	NA	NA	NA	NA			N
Ni	Post	0.094	0.235	0.016	5	9.40	N	Y
	Pre	0.010	0.011	0.009	2			N
Pb	Post	0.083	0.188	0.026	4	10.4	N	Y
	Pre	0.008	0.009	0.008	2			N
Ca	Post	366	856	197	9	1.71	Y	N
	Pre	214	386	76.9	13			N
K	Post	12.8	41.9	1.80	9	6.72	Y	N
	Pre	1.91	2.72	1.51	13			N
Li	Post	0.050	0.141	0.016	9	3.85	Y	N
	Pre	0.013	0.019	0.006	13			N
Mg	Post	51.6	87.2	35.6	9	1.55	Y	N
	Pre	33.4	45.5	19.2	13			N
Si	Post	38.5	99.6	4.47	9	6.95	Y	N
	Pre	5.54	12.6	3.19	13			N
Zn	Post	0.296	1.070	0.008	9	16.4	Y	N
	Pre	0.018	0.051	0.007	13			N

For the group with significantly different means for pre-storm vs post-storm flow concentrations and values above MCLs (Al, As, Ba, Cr, Fe, and Mn; Figure 6), most concentrations were above MCLs only for post-storm samples. However, As concentrations were all above the EPA primary MCLs even for pre-storm samples. Al, Fe, and Mn pre-storm concentrations were above EPA secondary MCLs for some samples but not all, whereas Ba and Cr pre-storm samples were all below the EPA primary MCLs. For post-storm samples, the majority of Al, As, Fe, and Mn concentrations were above the EPA primary and secondary MCLs, whereas Ba and Cr only had two-three samples above the limit. Mean concentrations for pre to post-storm comparisons increased for all of these metals, with the smallest percent increase for As and largest for Mn (Table 6).

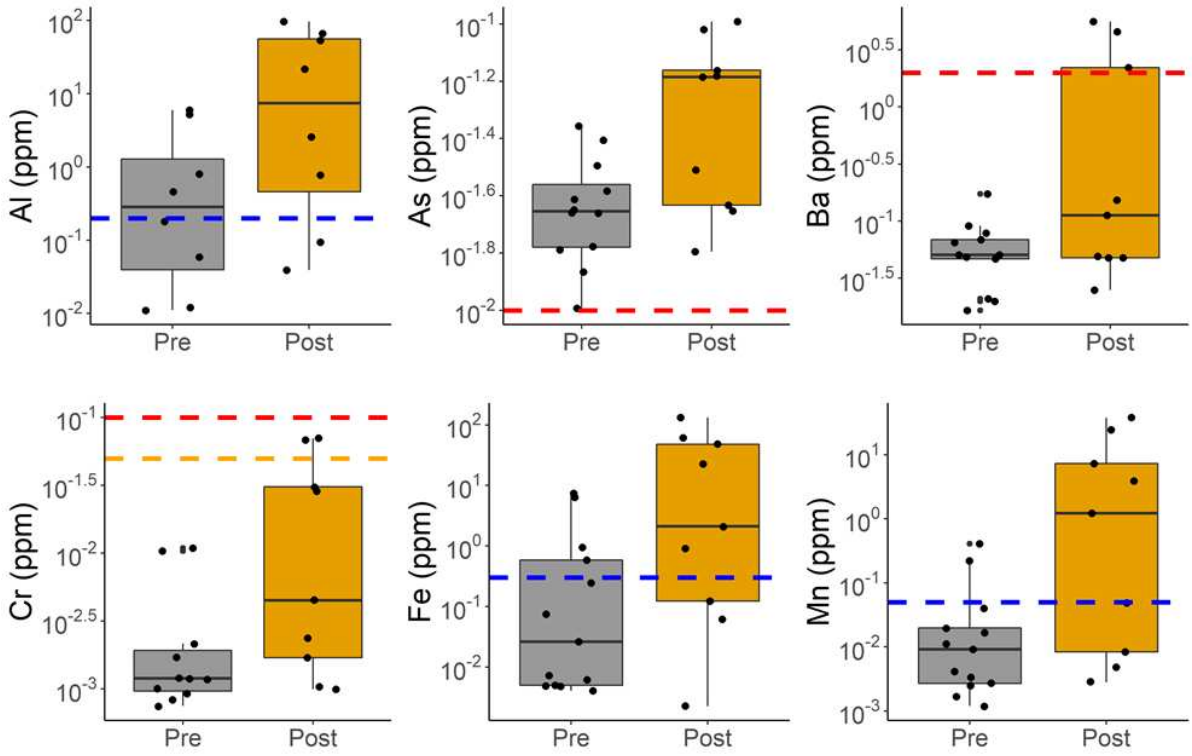

Figure 6: Metals with significant differences between pre-storm and post-storm concentrations and with some concentrations above MCLs. Red dashed lines are the MCL for EPA primary drinking water contaminant levels; blue dashed lines are the MCL for EPA secondary drinking water contaminant levels, and the orange line is the MCL for WHO drinking water standard. Note: MCL's are in Table A2

Be, Cd, Ni, and Pb all had post-storm concentrations above EPA or WHO drinking water standards (Figure 7), but the concentrations were not significantly different from pre- to post-storm samples because of small sample sizes; many of the samples had concentrations below detection limits. Cd was not detected at any site before a storm event. Other metals in this group did show detectable concentrations for pre-storm samples, but none of these samples were above any drinking water standard. This group of metals had the highest percent average increase to concentrations, but these numbers may not be very representative because of the small number of samples with detectable concentrations. Finally, Ca, K, Li, Mg, Si, and Zn all had significant

difference between pre-storm and post-storm concentrations (Figure 8). However, none of the metals in this group had concentrations above a drinking water standard.

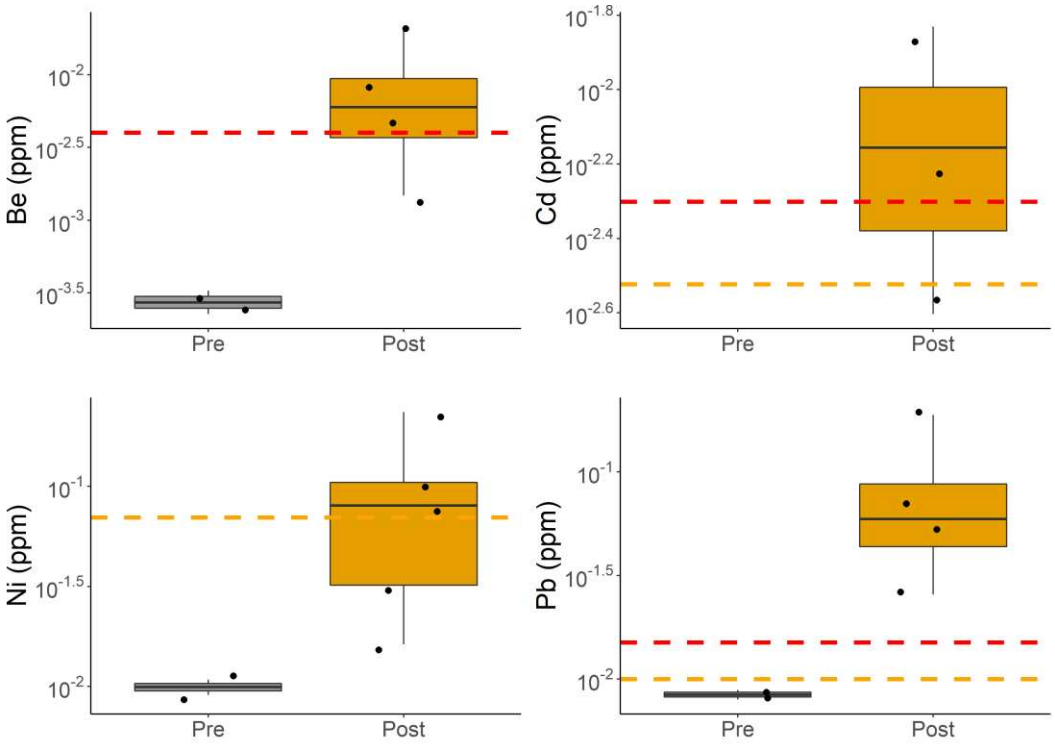

Figure 7: Metals without significant differences between pre- and post-storm concentrations with some concentrations above drinking water contaminant limits. Red dashed lines are the MCL for EPA primary drinking water standard, and the orange line is the MCL for WHO drinking water standard. Note: MCL's are in Table A2.

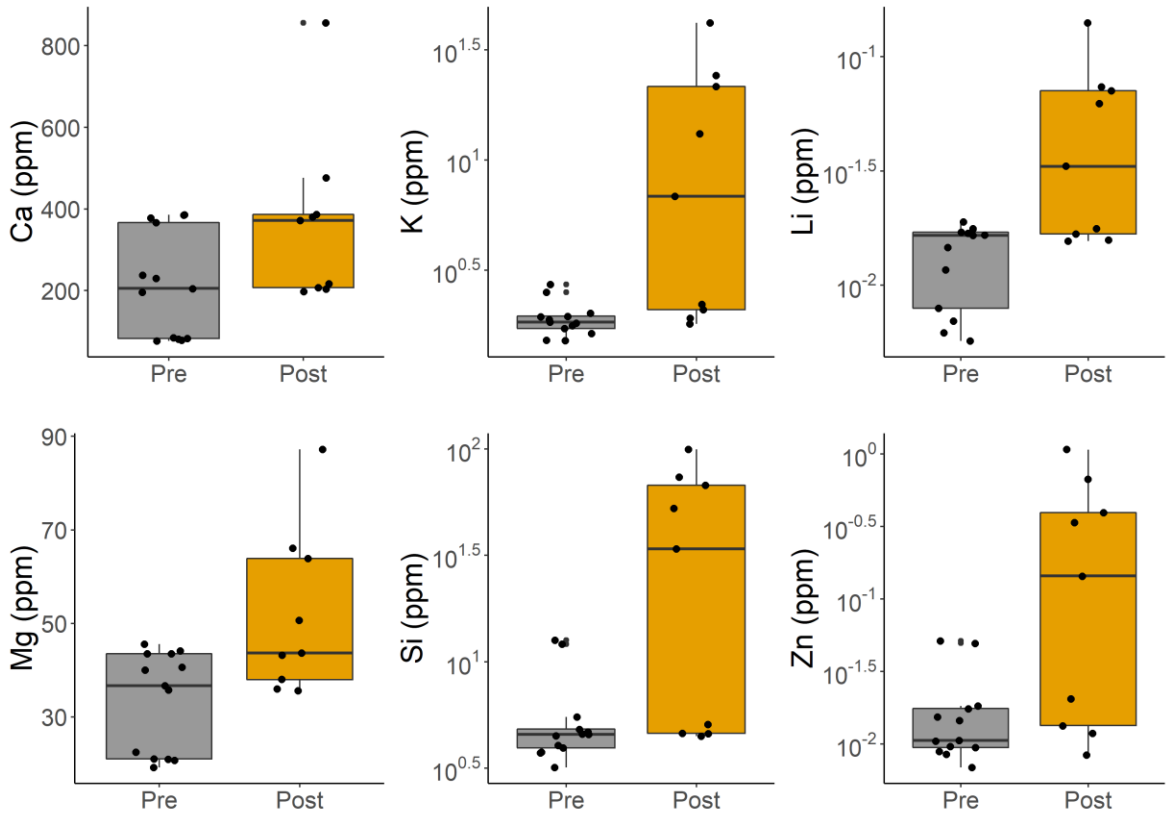

Figure 8: Metals with significant differences between pre-storm vs post-storm concentrations but with no concentrations above MCLs.

To identify potential drivers of stormflow metal concentrations, I conducted correlation analyses between metal concentrations and watershed/burn characteristics for all metals with significant differences between pre- and post-storm samples (Figures 9,10). In contrast to the baseflow samples, many of the stormflow samples had significant correlations with burn variables, in particular mean dNBR and percentage of watershed burned. Mean dNBR values for watersheds were positively and significantly correlated with concentrations of Al, As, Ba, Fe, Li, Mg, Si, and Zn. In contrast the percent of watershed burned was negatively correlated with metal concentrations, and these correlations were significant for all metals except Cr, Mg, and Ca. All metals except Cr had concentrations that were positively correlated with mean elevation,

precipitation, and drainage area but negatively correlated with change in elevation and slope. None of the correlations with soil types C or D were significant. Cr, Ca, and K also did not have significant correlations with any of the watershed or burn variables.

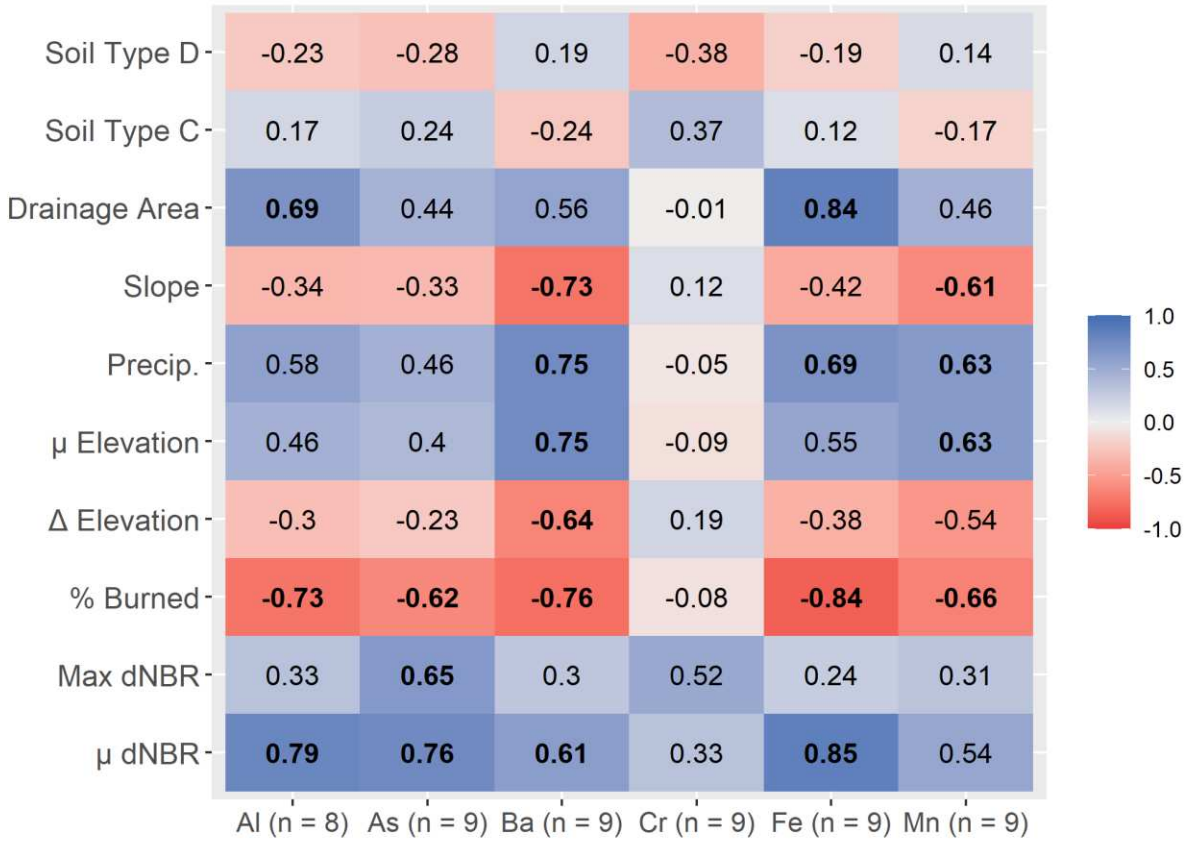

Figure 9: Correlation matrix between all watershed characteristics and burn variables vs group 1 storm event metal concentrations. Correlations are considered significant and bolded where Pearson correlation coefficients (r) are greater than 0.6.

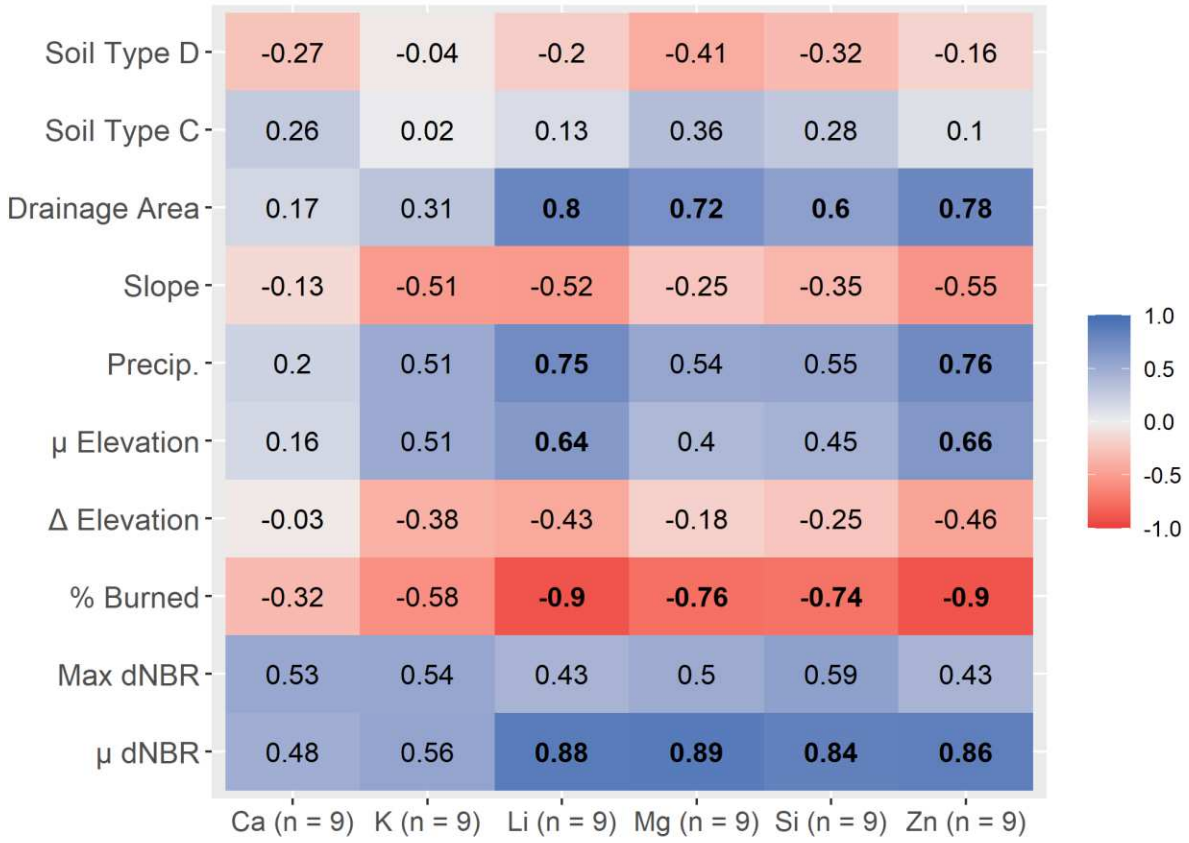

Figure 10: Correlation matrix between all watershed characteristics and burn variables vs group 3 storm event metal concentrations. Correlations are considered significant and bolded where Pearson correlation coefficients (r) are greater than 0.6.

5. DISCUSSION

The fire created altered hydrologic conditions that allowed higher metal concentrations to reach streams. During stormflow, many metal concentrations exceeded EPA and WHO maximum contaminant limits. The potential flow paths that could bring metals into streams are illustrated conceptually in Figure 11. The first path is during storm events, which increase mobilization of sediment-adsorbed metals as well as newly soluble metals from destruction of SOM (Figure 11a). Surface soil layers are greatly altered by wildfire intensity, which can release sequestered metals from SOM and clay minerals and prevent the formation of insoluble metal oxides and hydroxides through humic acid interactions (Kabata-Pendias 2012; Kaschl, Romheld, and Chen 2002). Loss of ground cover and decreased infiltration rates after wildfire can increase ash and sediment transport via surface overland flow and erosion from rain storms (Kampf et al. 2016b; Onda, Dietrich, and Booker 2008). The likelihood of surface erosion increases with greater burn severity (Abraham 2017; Kampf et al. 2016; Rhoades 2011), and this may explain why mean dNBR exhibited a strong ($r \sim 0.8$) positive correlation with metal concentrations for storm flow samples.

Both ash and sediments can be mobilized by overland flow and cause rapid transport of bound and dissolved metals to streams. This mechanism is supported by the elevated concentrations in storm flow samples for 12 of 28 analyzed metals (Al. As, Ba, Ca, Cr, Fe, K, Li, Mg, Mn, Si, Zn) at all of the sites with both pre- and post-stormflow samples. Concentrations of these metals were 1.5 – 145 times greater than pre-storm samples, indicating a strong role of storm runoff in transporting metals. Previous studies have reported that the major and trace

metals (As, Ca, Cu, Cd, Fe, Hg, K, Mg, Mn, Na, Pb, and Zn) are all found in ash, with Mn consistently having the highest concentration (Campos et al. 2016). All of these metals were elevated for post-storm samples from the 416 fire with the exception of Cu and Hg, indicating that the storm pulses flushed out ash deposits available for mobilization through surface erosion. Ca exhibited the highest concentrations (μ 366 ppm) in storm samples, while Mn had the largest increase (146x) from pre- to post-storm samples.

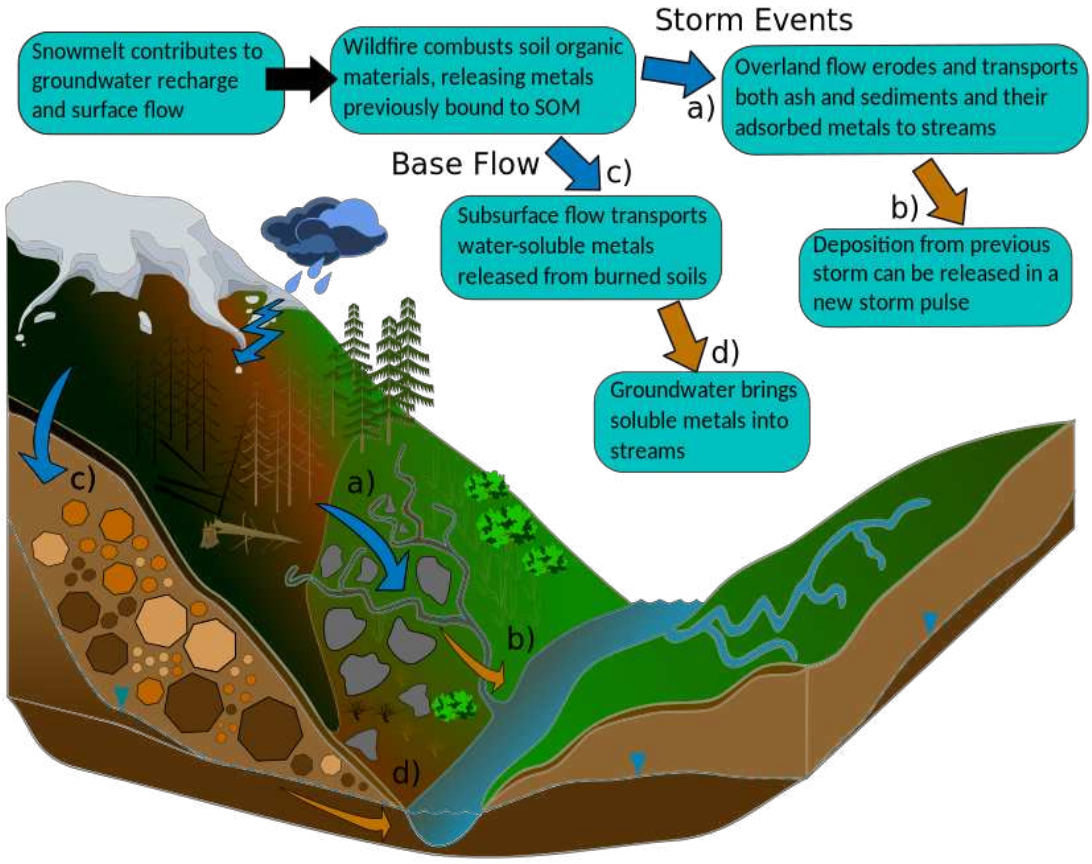

Figure 11: Conceptual diagram of the steps of metal transport in post-fire environments. The movement of arrows and processes are labeled a-d as well as color coded. Arrows indicate surface overland flow and subsurface interactions. Blue to orange arrows indicate higher metal contaminated flow before reaching a stream.

Three of the metals with high increases for stormflow (Al, Fe, and Mn; 18.9x, 24.6x, and 146x) also had significant differences between filtered and unfiltered samples at baseflow, with higher concentrations in the unfiltered samples. This suggests these metals can be bound to sediment, which may account for their substantial increases in concentration during storm events. Filtered vs. unfiltered comparisons were not available for stormflow samples because both pre- and post-storm samples were acid-digested. Upland surface erosion and overland flow are likely dominant causes of sediment-bound metal transport shortly after fire, although during storm pulses these sediments can be deposited in or near channels (Bodí et al. 2014; Kampf et al. 2016b; Wilson et al. 2018). These deposited sediments can then be re-mobilized during subsequent storms and snowmelt runoff (Figure 11b).

While metal concentrations were greatly elevated in stormflow samples relative to baseflow samples, baseflow at burned sites still did have higher metal concentrations than unburned sites. Nine metals had significant differences in metal concentrations relative to unburned baseflow; eight (As, Ca, K, Mg, Mo, Si, Sr, Zn) had concentrations that were 1.2 – 12 times greater than the unburned sites, and one (Ba) had lower concentrations that were 0.63 times lower than the unburned sites. Aside from Ba, which will be discussed later on, the increased metal concentrations at burned sites likely indicate that metals reached streams not only through surface erosion and transport but also through subsurface flow that transports soluble metals (Figure 11c,d).

Out of ten predictor variables that cover physical, edaphic, and burn characteristics of the measured watersheds, four variables (mean basin elevation, mean annual precipitation, change in elevation along the longest flow path and percentage of watershed burned) had high cross

correlations with each other and the highest correlations to metals concentration in streams. Percent watershed burned is highly correlated with precipitation and elevation variables because the lower elevation tributaries had greater percent burn than the higher elevation sampling sites. Unfortunately, this means it is not possible to separate the burn effect from the orographic effect on differences in metal concentrations. However, the multivariate analysis showed that percentage of watershed burned had the highest standardized beta coefficients for six of the metals (As, Ba, Mg, Mo, Si, Zn), which may be a stronger indication that the burn did increase baseflow metal concentrations.

In the absence of fire, overland flow in this environment is rare, with most water traveling through the subsurface before reaching streams. In spite of the increased overland flow post-fire, some studies have documented post-fire groundwater recharge increases as well (Bart and Tague 2017; Ebel 2013), possibly due to loss of root water uptake. Any water traveling through the subsurface before reaching streams would interact with subsurface geology. The altered physical and chemical changes to water chemistry post-fire can increase water-rock interaction and alter chemical weathering equilibria (Aiuppa et al. 2000; Maher 2010), which can increase mineral solubility and dissolve complexed metals in shallow subsurface flow and deeper groundwaters. In the study watersheds the sequence of shales, siltstone, mudstone, limestone and arkosic sandstone have a mix of clay minerals (kaolinite, illite, and smectite), feldspar, quartz, and metal oxides/hydroxides (Dayal 2017; Maslov et al. 2019). Potential pathways for metal mobilization in the subsurface are: (1) pH decreases from pyrite oxidation and interaction with nutrients (Houben et al. 2019; Murphy et al. 2020). (2) An acidification front in the unsaturated zone just above the water table. can form (Kjøller, Postma, and Larsen 2004). (3) Deeper subsurface flows encounter more reductive conditions creating greater metal solubility

(Campbell et al. 2006; Erbs et al. 2010). (4) Post-fire alkaline soils cause humic acid to dissolve and suppress the formation insoluble metal hydroxides (González-Pérez et al. 2004; Heydari et al. 2017; Spark, Wells, and Johnson 1997). (5) Destruction of soil o-horizon mobilizes SOM and weakly bound metals (Bodí et al. 2014; Certini 2005; González-Pérez et al. 2004; Koyama et al. 2012). Although this study shows increased metals during baseflow at burned sites and a strong positive correlation to percentage of watershed burned, more comprehensive geochemical investigations would need to be conducted to determine the geochemical transformations between the soil horizon, unsaturated zone, and saturated zone.

Of the metals explored in baseflow analyses, Ba, Si, and Zn concentrations were least correlated with the other metals. Ba actually had inverse directions of relationships to the predictor variables compared to other metals. Ba has strong uptake by vegetation, so potentially more was contained within ash during the fire, leading to the negative relationship ($r = -0.72$) with percentage of watershed burned (Isley and Taylor 2020). There was a relatively small percent change in baseflow samples of 20% for Si, and it was also on the boarder of significance ($p = 0.055$) in showing a difference in filtered and unfiltered samples. This indicates Si complexes have low solubility, so only those that are weakly bound such as poorly crystalized Si minerals or Si sediment surfaces are likely to be released into water. Zn had distinct patterns from the other metals, due the high variability of concentrations for each site. This variability in Zn concentrations may have been caused by concentrations being close to the limit of detection for the ICP ~ 0.005 ppm. The 16.4x increase for post-storm samples in Zn concentrations indicate most of the Zn in this system is readily mobilized in ash, post-fire litter, or eroded sediment.

Water-quality impacts of fire will continue to be a concern with the prevalence of fires

across the western US and other parts of the world. Elevated nutrients, organic carbon, and sediment are common in post-fire streams and may persist for 1-15 years after a fire (Abraham et al. 2017; Murphy et al. 2020). Elevated metal concentrations may also persist for 1-5 years after fire, especially during storm pulses (Murphy et al. 2020). Recently trace metals have been the focus of post-fire water-quality studies, and many have reported metal concentrations that border or exceed drinking water quality standards (Abraham et al. 2017; Murphy et al. 2020; Rust et al. 2019). Similarly I found that As concentrations exceeded MCLs during baseflow, and Al, As, Ba, Be, Cd, Cr, Fe, Mn, Ni, and Pb exceeded MCLs during stormflow. Depending on vegetation recovery and groundwater recharge rates these metals could remain elevated for years. Many watersheds that provide an essential water supply have also experienced decades or fire suppression in the Western US, making them vulnerable to larger and higher severity fires (Hessburg et al. 2019; Rodman et al. 2019; Westerling et al. 2006). Increased precipitation and higher temperatures from climate change could negatively impact metal mobilization in post-fire environments as well (Liu, Stanturf, and Goodrick 2010). Reduced snowpack persistence and increased storm frequency can create earlier stream flows and more storm flow events with impacted water quality in post-fire environments (Peñuelas et al. 2017; Stewart 2009). Murphy (2020) reported substantial overlap of important surface water supply, high wildfire potential and legacy mine locations in the Western US. Elevated metal concentrations in post-fire environments are a complex geochemical and hydrologic problem that could be compounded by a changing climate and historic mining waste. It is imperative for land use managers, water treatment facilities, and related organizations to understand the release of metals into post-fire streams, so informed decisions about treatment, assessment, and protection of vulnerable watersheds can be made.

6. CONCLUSIONS

With wildfire frequency, size, and intensity on the rise it is paramount to understand their environmental impact, so we may better respond to or prevent degradation of our natural resources. The mobilization of metals in post-fire environments is driven by a set of complex ecological, geochemical, hydrologic and fire processes. Our study provides insight into metal transport processes at the river and tributary scale for baseflow and stormflow. For baseflow the strongest relationship to metal concentrations was percentage of watershed burned ($r \sim 0.8$). Although baseflow metal concentrations did not exceed most water quality standards, the 2.21x average increase in metal concentrations relative to unburned conditions are still of concern and may impact water treatment facilities. The highly toxic As exhibited concentrations above the EPA primary drinking water MCL even for baseflow. Impacts on water quality were much greater during storm events where concentrations increased by more than 20.6x on average. Al, As, Ba, Be, Cd, Cr, Fe, Mn, Ni, and Pb all had stormflow concentrations above an EPA or WHO drinking water MCL. Although storm samples were limited, metal concentrations were correlated with watershed burn severity ($r \sim 0.8$), indicating elevated metal concentrations likely came from areas with higher burn severity that generated surface overland flow and erosion. This study confirms increased metal concentrations are commonplace in post-fire streams, particularly where surface erosion transports ash and sediment to streams, and results also demonstrate that fire can also elevate metal concentrations in baseflow. Because of the water quality concerns associated with elevated metals, future work should examine metal concentrations for more fires

and add in comprehensive geochemical analyses to better understand what mechanisms control the release of metals to watersheds within a burn area.

BIBLIOGRAPHY

Abraham, Joji, Kim Dowling, and Singarayer Florentine. 2017. "Risk of Post-Fire Metal Mobilization into Surface Water Resources: A Review." *Science of The Total Environment* 599–600:1740–55.

Aiuppa, Alessandro, Patrick Allard, Walter D'Alessandro, Agnes Michel, Francesco Parello, Michel Treuil, and Mariano Valenza. 2000. "Mobility and Fluxes of Major, Minor and Trace Metals during Basalt Weathering and Groundwater Transport at Mt. Etna Volcano (Sicily)." *Geochimica et Cosmochimica Acta* 64(11):1827–41.

Anon. 2017. *Guidelines for Drinking-Water Quality: Fourth Edition Incorporating the First Addendum*. World Health Organization.

Anon. n.d. "WRCC." Retrieved October 17, 2020 (https://wrcc.dri.edu/).

Bart, Ryan R. and Christina L. Tague. 2017. "The Impact of Wildfire on Baseflow Recession Rates in California." *Hydrological Processes* 31(8):1662–73.

Barton, Kamil. 2020. "MuMIn: Multi-Model Inference."

Biester, H., G. Muller, H. F. Scholer¨¨, and Scholer¨ Scholer¨¨. 2002. *Binding and Mobility of Mercury in Soils Contaminated by Emissions from Chlor-Alkali Plants*. Vol. 284.

Biswas, Abir, Joel D. Blum, Bjoern Klaue, and Gerald J. Keeler. 2007. "Release of Mercury from Rocky Mountain Forest Fires." *Global Biogeochemical Cycles* 21(1).

Bodí, Merche B., Deborah A. Martin, Victoria N. Balfour, Cristina Santín, Stefan H. Doerr, Paulo Pereira, Artemi Cerdà, and Jorge Mataix-Solera. 2014. "Wildland Fire Ash: Production, Composition and Eco-Hydro-Geomorphic Effects." *Earth Science Reviews* 130:103–27.

Brown, Thomas C., Michael T. Hobbins, and Jorge A. Ramirez. 2008. "Spatial Distribution of Water Supply in the Coterminous United States." *Journal of the American Water Resources Association* 44(6):1474–87.

Campbell, Kate M., Davin Malasarn, Chad W. Saltikov, Dianne K. Newman, and Janet G. Hering. 2006. “Simultaneous Microbial Reduction of Iron(III) and Arsenic(V) in Suspensions of Hydrous Ferric Oxide.” *Environmental Science and Technology* 40(19):5950–55.

Campos, Isabel, Nelson Abrantes, Jan Jacob Keizer, Carlos Vale, and Patrícia Pereira. 2016. “Major and Trace Elements in Soils and Ashes of Eucalypt and Pine Forest Plantations in Portugal Following a Wildfire.” *Science of the Total Environment* 572:1363–76.

Certini, Giacomo. 2005. “Effects of Fire on Properties of Forest Soils: A Review.” *Oecologia* 143(1):1–10.

Clarke, Peter J., Kirsten E. J. Knox, and Damian Butler. 2013. “Fire, Soil Fertility and Delayed Seed Release: A Community Analysis of the Degree of Serotiny.” *Evolutionary Ecology* 27(2):429–43.

Dayal, Anurodh Mohan. 2017. *Shale*. Elsevier Inc.

Debano, Leonard F. 1990. “THE EFFECT OF FIRE ON SOIL PROPERTIES.” *General Technical Report USFS*.

Ebel, Brian A. 2013. “Simulated Unsaturated Flow Processes after Wildfire and Interactions with Slope Aspect.” *Water Resources Research* 49(12):8090–8107.

Eckel, Edwin B. 1949. *Geology and Ore Deposits of the La Plata District, Colorado*.

Erbs, Jasmine J., Thelma S. Berquó, Brian C. Reinsch, Gregory V. Lowry, Subir K. Banerjee, and R. Lee Penn. 2010. “Reductive Dissolution of Arsenic-Bearing Ferrihydrite.” *Geochimica et Cosmochimica Acta* 74(12):3382–95.

Fox, John and Sanford Weisberg. 2019. *An {R} Companion to Applied Regression*. Third. Thousand Oaks {CA}: Sage.

Gallaher, B., Koch, R., Mullen, K. 2002. *Quality of Storm Water Runoff at Los Alamos National Laboratory in 2000*.

Gonzales, D, Stahr, D.W., and Kirkham, R. W. 2004. “Geologic Map of the Hermosa Quadrangle, La Plata County, Colorado.” *Colorado Geological Survey* (Open-File Report

OF02-01):1:24,000.

González-Pérez, José A., Francisco J. González-Vila, Gonzalo Almendros, and Heike Knicker. 2004. “The Effect of Fire on Soil Organic Matter - A Review.” *Environment International* 30(6):855–70.

Hansen, Lindsey. 2019. “416 Fire Burned Area Emergency Response (BAER) Executive Summary.”

Hessburg, Paul F., Carol L. Miller, Sean A. Parks, Nicholas A. Povak, Alan H. Taylor, Philip E. Higuera, Susan J. Prichard, Malcolm P. North, Brandon M. Collins, Matthew D. Hurteau, Andrew J. Larson, Craig D. Allen, Scott L. Stephens, Hiram Rivera-Huerta, Camille S. Stevens-Rumann, Lori D. Daniels, Ze’ev Gedalof, Robert W. Gray, Van R. Kane, Derek J. Churchill, R. Keala Hagmann, Thomas A. Spies, C. Alina Cansler, R. Travis Belote, Thomas T. Veblen, Mike A. Battaglia, Chad Hoffman, Carl N. Skinner, Hugh D. Safford, and R. Brion Salter. 2019. “Climate, Environment, and Disturbance History Govern Resilience of Western North American Forests.” *Frontiers in Ecology and Evolution* 7:239.

Heydari, M., A. Rostamy, F. Najafi, and D. C. Dey. 2017. “Effect of Fire Severity on Physical and Biochemical Soil Properties in Zagros Oak (Quercus Brantii Lindl.) Forests in Iran.” *Journal of Forestry Research* 28(1):95–104.

Hoover, Katie. 2018. “Wildfire Statistics.”

Hothorn, Torsten, Kurt Hornik, Mark A. van de Wiel, and Achim Zeileis. 2008. “Implementing a Class of Permutation Tests: The {coin} Package.” *Journal of Statistical Software* 28(8):1–23.

Houben, Georg J., Stephan Kaufhold, Jan Dietel, Herbert Röhm, Jens Gröger-Trampe, and Jürgen Sander. 2019. “Investigation of the Source of Acidification in an Aquifer in Northern Germany.” *Environmental Earth Sciences* 78(3):73.

Isley, Cynthia Faye and Mark Patrick Taylor. 2020. “Atmospheric Remobilization of Natural and Anthropogenic Contaminants during Wildfires.” *Environmental Pollution* 267:115400.

Jolly, W. Matt, Mark A. Cochrane, Patrick H. Freeborn, Zachary A. Holden, Timothy J. Brown, Grant J. Williamson, and David M. J. S. Bowman. 2015. “Climate-Induced Variations in

Global Wildfire Danger from 1979 to 2013." *Nature Communications* 6(1):7537.

Kabata-Pendias, Alina. 2012. *Trace Elements in Soils and Plants*. 4th ed.

Kampf, Stephanie K., Daniel J. Brogan, Sarah Schmeer, Lee H. MacDonald, and Peter A. Nelson. 2016a. "How Do Geomorphic Effects of Rainfall Vary with Storm Type and Spatial Scale in a Post-Fire Landscape?" *Geomorphology* 273:39–51.

Kampf, Stephanie K., Daniel J. Brogan, Sarah Schmeer, Lee H. MacDonald, and Peter A. Nelson. 2016b. "How Do Geomorphic Effects of Rainfall Vary with Storm Type and Spatial Scale in a Post-Fire Landscape?" *Geomorphology* 273:39–51.

Kaschl, Arno, Volker Romheld, and Yona Chen. 2002. *The Influence of Soluble Organic Matter from Municipal Solid Waste Compost on Trace Metal Leaching in Calcareous Soils*. Vol. 291.

Kjøller, Claus, Dieke Postma, and Flemming Larsen. 2004. "Groundwater Acidification and the Mobilization of Trace Metals in a Sandy Aquifer." *Environmental Science and Technology* 38(10):2829–35.

Kong, Jian-jian, Jian Yang, and Edith Bai. 2018. "Long-Term Effects of Wildfire on Available Soil Nutrient Composition and Stoichiometry in a Chinese Boreal Forest." *Science of The Total Environment* 642:1353–61.

Koyama, Akihiro, Kirsten Stephan, and Kathleen L. Kavanagh. 2012. "Fire Effects on Gross Inorganic N Transformation in Riparian Soils in Coniferous Forests of Central Idaho, USA: Wildfires v. Prescribed Fires." *International Journal of Wildland Fire* 21(1):69.

Leak, M., Passuello, R., Tyler, B. 2003. "I've Seen Fire. I've Seen Rain. I've Seen Muddy Waters That I Thought Would Never Clear Again." *Waterworks* 6:38–44.

Lenth, Russell. 2020. "Emmeans: Estimated Marginal Means, Aka Least-Squares Means."

Liu, Yongqiang, John Stanturf, and Scott Goodrick. 2010. "Trends in Global Wildfire Potential in a Changing Climate." *Forest Ecology and Management* 259(4):685–97.

Lyon, Peggy, Denise Culver, Maggie March, and Lauren Hall. 2003. "San Juan County Biological Assessment." (March).

Maher, K. 2010. “The Dependence of Chemical Weathering Rates on Fluid Residence Time.”

Maslov, A. V., V. N. Podkovyrov, E. Z. Gareev, and A. D. Nozhkin. 2019. “Synrift Sandstones and Mudstones: Bulk Chemical Composition and Position in Some Discriminant Paleogeodynamic Diagrams.” *Lithology and Mineral Resources* 54(5):390–411.

Matichenkov, V. V. and E. A. Bocharnikova. 2001. “Chapter 13 The Relationship between Silicon and Soil Physical and Chemical Properties.” *Studies in Plant Science* 8(C):209–19.

Miller, J. D., H. D. Safford, M. Crimmins, and A. E. Thode. 2009. “Quantitative Evidence for Increasing Forest Fire Severity in the Sierra Nevada and Southern Cascade Mountains, California and Nevada, USA.” *Ecosystems* 12(1):16–32.

Murphy, Sheila F., R. Blaine McCleskey, Deborah A. Martin, Jo Ann M. Holloway, and Jeffrey H. Writer. 2020. “Wildfire-Driven Changes in Hydrology Mobilize Arsenic and Metals from Legacy Mine Waste.” *Science of the Total Environment* 743:140635.

Norouzi, Mehdi and Hassan Ramezanpour. 2013. “Effect of Fire on Chemical Forms of Iron and Manganese in Forest Soils of Iran.” *Environmental Forensics* 14(2):169–77.

Onda, Yuichi, William E. Dietrich, and Fred Booker. 2008. “Evolution of Overland Flow after a Severe Forest Fire, Point Reyes, California.” *Catena* 72(1):13–20.

Peñuelas, Josep, Jordi Sardans, Iolanda Filella, Marc Estiarte, Joan Llusià, Romà Ogaya, Jofre Carnicer, Mireia Bartrons, Albert Rivas-Ubach, Oriol Grau, Guille Peguero, Olga Margalef, Sergi Pla-Rabés, Constantí Stefanescu, Dolores Asensio, Catherine Preece, Lei Liu, Aleixandre Verger, Adrià Barbeta, Ander Achotegui-Castells, Albert Gargallo-Garriga, Dominik Sperlich, Gerard Farré-Armengol, Marcos Fernández-Martínez, Daijun Liu, Chao Zhang, Ifigenia Urbina, Marta Camino-Serrano, Maria Vives-Ingla, Benjamin Stocker, Manuela Balzarolo, Rossella Guerrieri, Marc Peaucelle, Sara Marañón-Jiménez, Kevin Bórnez-Mejías, Zhaobin Mu, Adrià Descals, Alejandro Castellanos, Jaume Terradas, Josep Peñuelas, Jordi Sardans, Iolanda Filella, Marc Estiarte, Joan Llusià, Romà Ogaya, Jofre Carnicer, Mireia Bartrons, Albert Rivas-Ubach, Oriol Grau, Guille Peguero, Olga Margalef, Sergi Pla-Rabés, Constantí Stefanescu, Dolores Asensio, Catherine Preece, Lei Liu, Aleixandre Verger, Adrià Barbeta, Ander Achotegui-Castells, Albert Gargallo-Garriga,

Dominik Sperlich, Gerard Farré-Armengol, Marcos Fernández-Martínez, Daijun Liu, Chao Zhang, Ifigenia Urbina, Marta Camino-Serrano, Maria Vives-Ingla, Benjamin D. Stocker, Manuela Balzarolo, Rossella Guerrieri, Marc Peaucelle, Sara Marañón-Jiménez, Kevin Bórnez-Mejías, Zhaobin Mu, Adrià Descals, Alejandro Castellanos, and Jaume Terradas. 2017. "Impacts of Global Change on Mediterranean Forests and Their Services." *Forests* 8(12):463.

Pereira, Paulo, Xavier Úbeda, and Deborah A. Martin. 2012. "Fire Severity Effects on Ash Chemical Composition and Water-Extractable Elements." *Geoderma* 191:105–14.

Reis, Ana Teresa, João Pedro Coelho, Isabel Rucandio, Christine M. Davidson, Armando C. Duarte, and Eduarda Pereira. 2015. "Thermo-Desorption: A Valid Tool for Mercury Speciation in Soils and Sediments?" *Geoderma* 237–238:98–104.

Rhoades, Charles C., Deborah Entwistle, and Dana Butler. 2011. "The Influence of Wildfire Extent and Severity on Streamwater Chemistry, Sediment and Temperature Following the Hayman Fire, Colorado." *International Journal of Wildland Fire* 20(3):430–42.

Rodman, Kyle C., Thomas T. Veblen, Sara Saraceni, and Teresa B. Chapman. 2019. "Wildfire Activity and Land Use Drove 20th-Century Changes in Forest Cover in the Colorado Front Range." *Ecosphere* 10(2):e02594.

RUAN, Xin-Ling, Gan-Lin ZHANG, Liu-Jian NI, and Yue HE. 2008. "Distribution and Migration of Heavy Metals in Undisturbed Forest Soils: A High Resolution Sampling Method." *Pedosphere* 18(3):386–93.

Rust, Ashley J., Samuel Saxe, John Mccray, Charles C. Rhoades, and Terri S. Hogue. 2019. "Evaluating the Factors Responsible for Post-Fire Water Quality Response in Forests of the Western USA."

Ryan, Sandra E., Kathleen A. Dwire, and Mark K. Dixon. 2011. "Impacts of Wildfire on Runoff and Sediment Loads at Little Granite Creek, Western Wyoming." *Geomorphology* 129(1–2):113–30.

Shcherbov, B. L. 2012. "The Role of Forest Floor in Migration of Metals and Artificial Nuclides during Forest Fires in Siberia." *Contemporary Problems of Ecology* 5(2):191–99.

Smith, Hugh G., Gary J. Sheridan, Patrick N. J. Lane, Petter Nyman, and Shane Haydon. 2011. "Wildfire Effects on Water Quality in Forest Catchments: A Review with Implications for Water Supply." *Journal of Hydrology* 396(1–2):170–92.

Someshwar, Arun V. 1996. "Wood and Combination Wood-Fired Boiler Ash Characterization." *Journal of Environment Quality* 25(5):962.

Spark, K. M., J. D. Wells, and B. B. Johnson. 1997. "The Interaction of a Humic Acid with Heavy Metals." *Australian Journal of Soil Research* 35(1):89–101.

Steven, T.A., Lipman, P.W., Hail, W.J., Barker, Fred, and Luedke, R. G. 1974. "Geologic Map of the Durango Quadrangle, Southwestern Colorado." *U.S. Geological Survey* (Miscellaneous Investigations Series Map I-764):1:250,000.

Stewart, Iris T. 2009. "Changes in Snowpack and Snowmelt Runoff for Key Mountain Regions." *Hydrological Processes* 23(1):78–94.

Townsend, Simon A. and Michael M. Douglas. 2004. "The Effect of a Wildfire on Stream Water Quality and Catchment Water Yield in a Tropical Savanna Excluded from Fire for 10 Years (Kakadu National Park, North Australia)." *Water Research* 38(13):3051–58.

Tubana, Brenda S., Tapasya Babu, and Lawrence E. Datnoff. 2016. "A Review of Silicon in Soils and Plants and Its Role in US Agriculture." *Soil Science* 181(9–10):1.

USDA Forest Service. 2007. *Soil Survey of Animas-Dolores Area, Colorado Parts of Archuleta, Dolores, Hinsdale, La Plata, Montezuma, San Juan, and San Miguel Counties*.

USDA Forest Service. 2014. "Forest Inventory and Analysis Data: Fiscal Year 2014 Business Report." (August).

USGS. 2016. "The StreamStats Program."

Westerling, A. L., H. G. Hidalgo, D. R. Cayan, and T. W. Swetnam. 2006. "Warming and Earlier Spring Increase Western U.S. Forest Wildfire Activity." *Science* 313(5789):940–43.

White, Ian, Alan Wade, Martin Worthy, Norm Mueller, Trevor Daniell, and Robert Wasson. 2006. "The Vulnerability of Water Supply Catchments to Bushfires: Impacts of the January 2003 Wildfires on the Australian Capital Territory." *Australasian Journal of Water*

Resources 10(2):179–94.

Williams, A. Park, Craig D. Allen, Constance I. Millar, Thomas W. Swetnam, Joel Michaelsen, Christopher J. Still, and Steven W. Leavitt. 2010. "Forest Responses to Increasing Aridity and Warmth in the Southwestern United States." *Proceedings of the National Academy of Sciences of the United States of America* 107(50):21289–94.

Wilson, Codie, Stephanie K. Kampf, Joseph W. Wagenbrenner, and Lee H. MacDonald. 2018. "Rainfall Thresholds for Post-Fire Runoff and Sediment Delivery from Plot to Watershed Scales." *Forest Ecology and Management* 430:346–56.

APPENDICES

Table A1 Water chemistry results for all burned (n = 37) and unburned (n = 5) sites.

		Concentration (ppm)				Burn > Control
		Mean	Max	Min	Std. Dev.	
ANC	Burn	3919	5972	1188	1053	Y
	Control	2815	3589	1931	706	
Ca	Burn	115	292	39	74	Y
	Control	59	78	35	18	
Cl	Burn	0.88	2.01	0.27	0.44	Y
	Control	0.37	0.60	0.22	0.16	
DIN	Burn	0.18	0.57	0.03	0.14	Y
	Control	0.06	0.16	0.00	0.06	
DOC	Burn	1.60	4.57	0.78	0.73	N
	Control	2.32	4.58	1.05	1.35	
DON	Burn	0.07	0.43	0.00	0.10	N
	Control	0.20	0.86	-0.01	0.37	
DTN	Burn	0.25	0.90	0.06	0.20	N
	Control	0.26	0.90	0.06	0.36	
EC	Burn	844	2201	318	556	Y
	Control	304	352	210	56	
F	Burn	0.29	3.16	0.01	0.62	Y
	Control	0.11	0.20	0.00	0.09	
K	Burn	1.37	3.22	0.62	0.57	Y
	Control	0.59	0.98	0.16	0.29	
Mg	Burn	25.4	50.9	7.5	12.9	Y
	Control	4.0	10.8	1.9	3.8	
Na	Burn	4.73	7.23	2.78	1.32	Y
	Control	2.32	3.67	0.49	1.18	
NH4	Burn	0.02	0.14	0.00	0.03	Y
	Control	0.01	0.02	0.00	0.01	
NO3	Burn	0.75	2.51	0.13	0.60	Y
	Control	0.21	0.64	0.00	0.26	
pH	Burn	8.3	8.7	8.1	0.2	-
	Control	8.3	8.5	8.1	0.1	
PO4	Burn	0.02	0.73	0.00	0.12	N
	Control	0.43	2.17	0.00	0.97	
SO4	Burn	196	742	4	238	Y
	Control	6.4	15.8	3.1	5.3	

Table A2: Table of MCL's for the EPA and WHO

	Concentration (ppm)		
	EPA		WHO
	Primary	Secondary	
Ag		0.1	
Al		0.05	
As	0.01		
Ba	2		
Be	0.004		
Cd	0.005		0.003
Cl		250	
Cr	0.1		0.05
Cu	1.3		2
Cn	0.2		
F	4		
Fe		0.3	
Mg		0.05	
Mn			0.4
Ni			0.07
Pb	0.015		0.01
Hg	0.002		0.001
Sb	0.006		
Zn		5	3

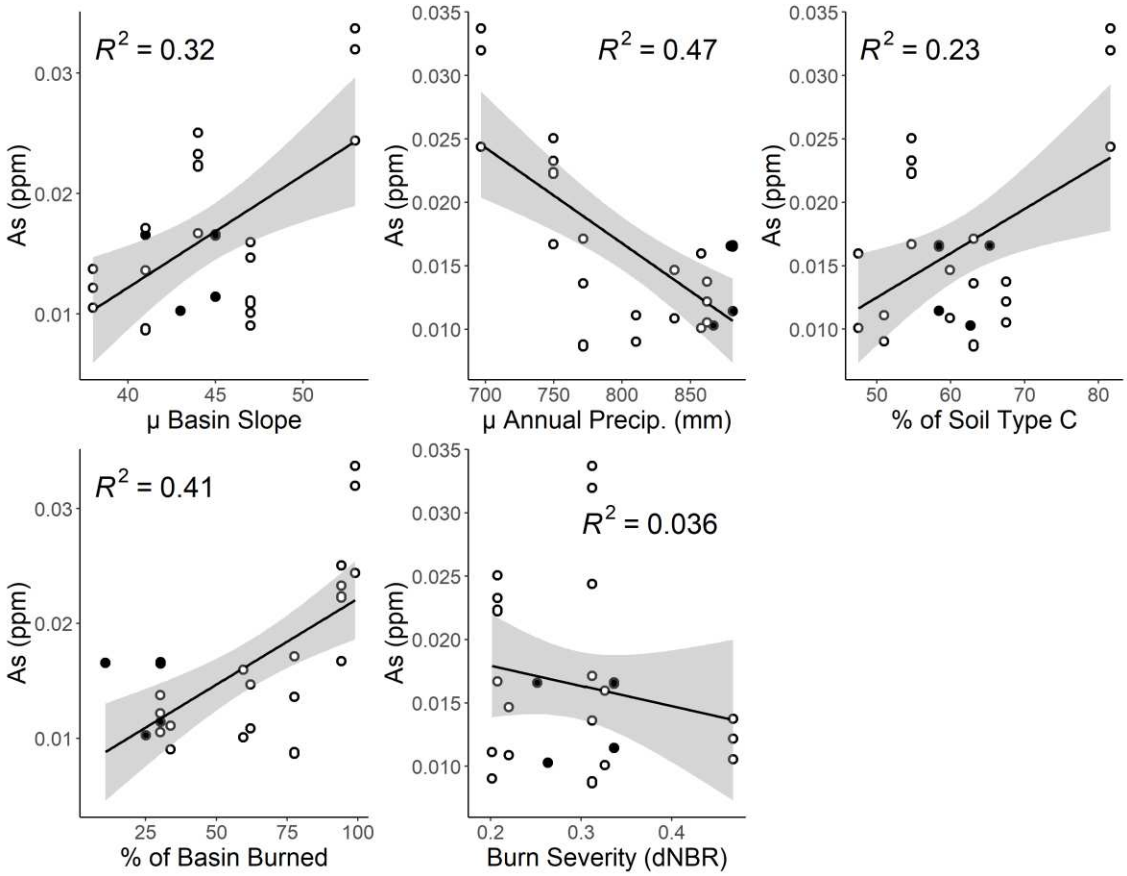

Figure A1: Linear relationships for watershed and burn characteristics for As, baseflow filtered (n = 26). Closed dots represent Hermosa Creek samples, and open dots represent tributary stream samples. The grey shape shows the standard error with 95% confidence. Coefficient of determination (R^2) is also shown.

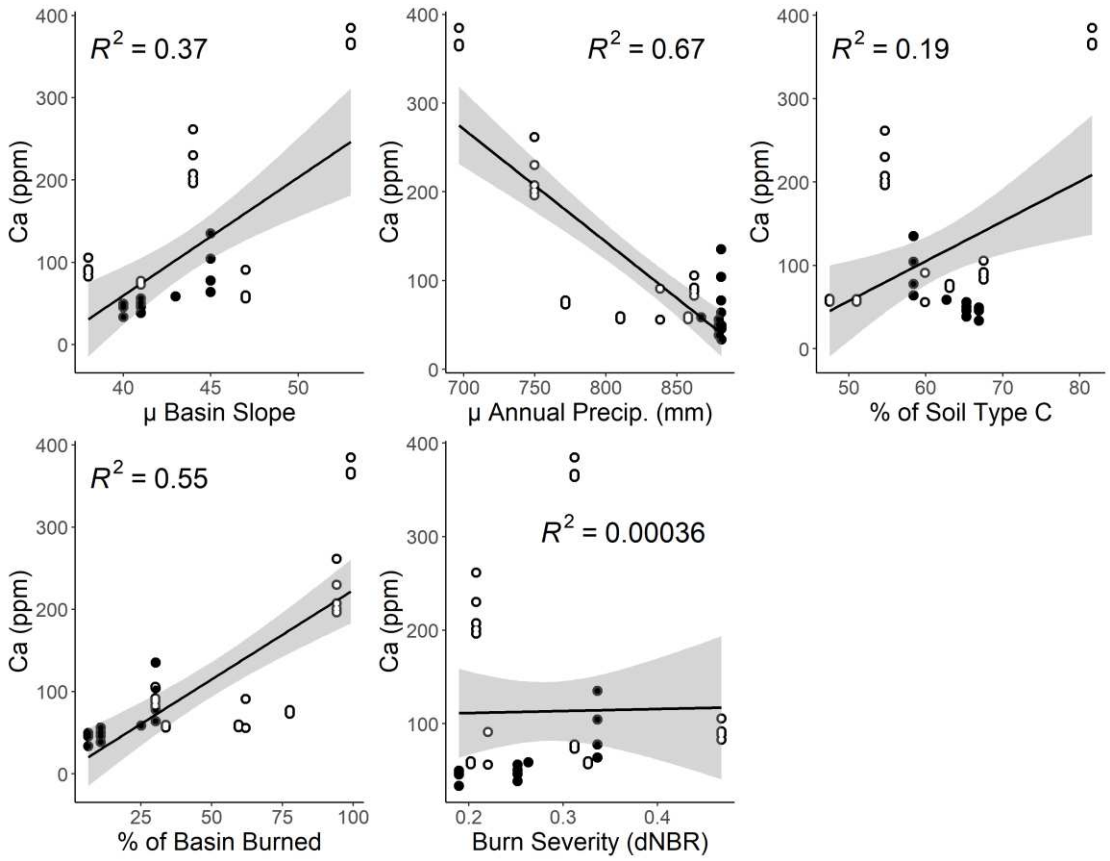

Figure A2: Linear relationships for watershed and burn characteristics for Ca, baseflow filtered (n = 37). Closed dots represent Hermosa Creek samples, and open dots represent tributary stream samples. The grey shape shows the standard error with 95% confidence. Coefficient of determination (R^2) is also shown.

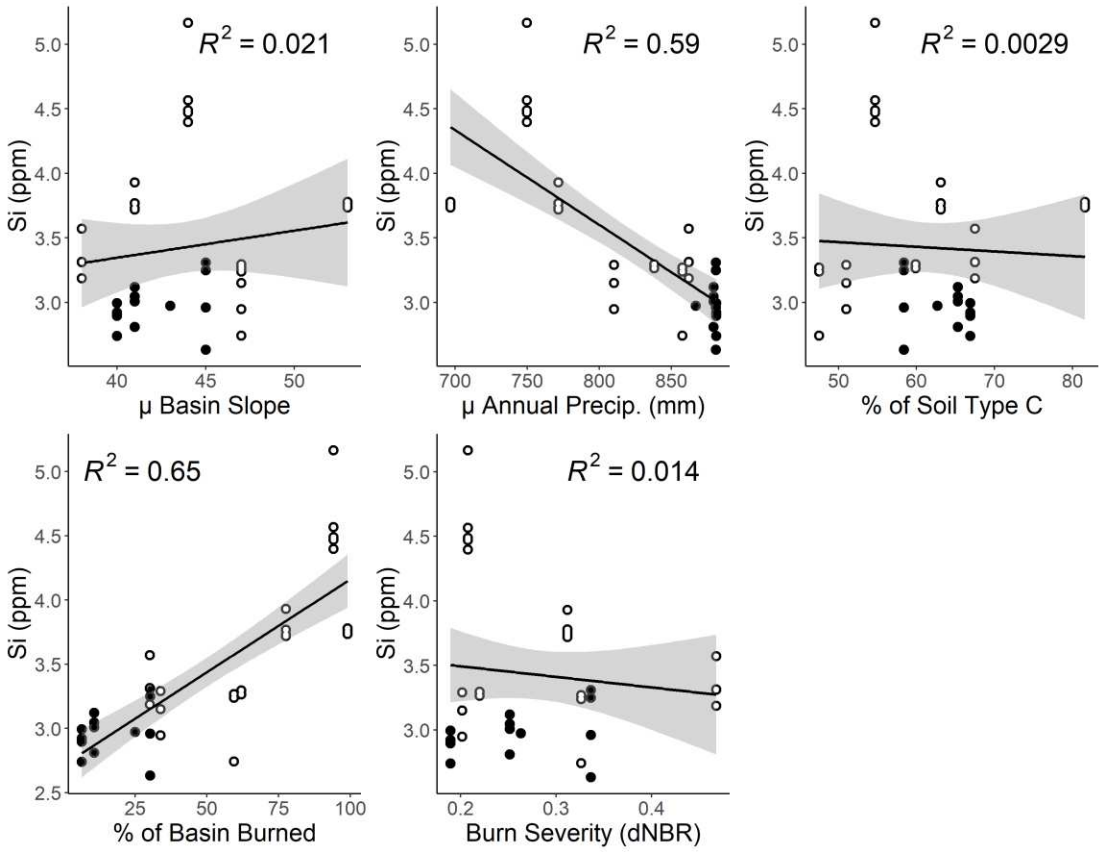

Figure A3: Linear relationships for watershed and burn characteristics for Si, baseflow filtered (n = 37). Closed dots represent Hermosa drainages and open dots represent tributary drainages. The grey shape shows the standard error with 95% confidence. Coefficient of determination (R^2) is also shown.

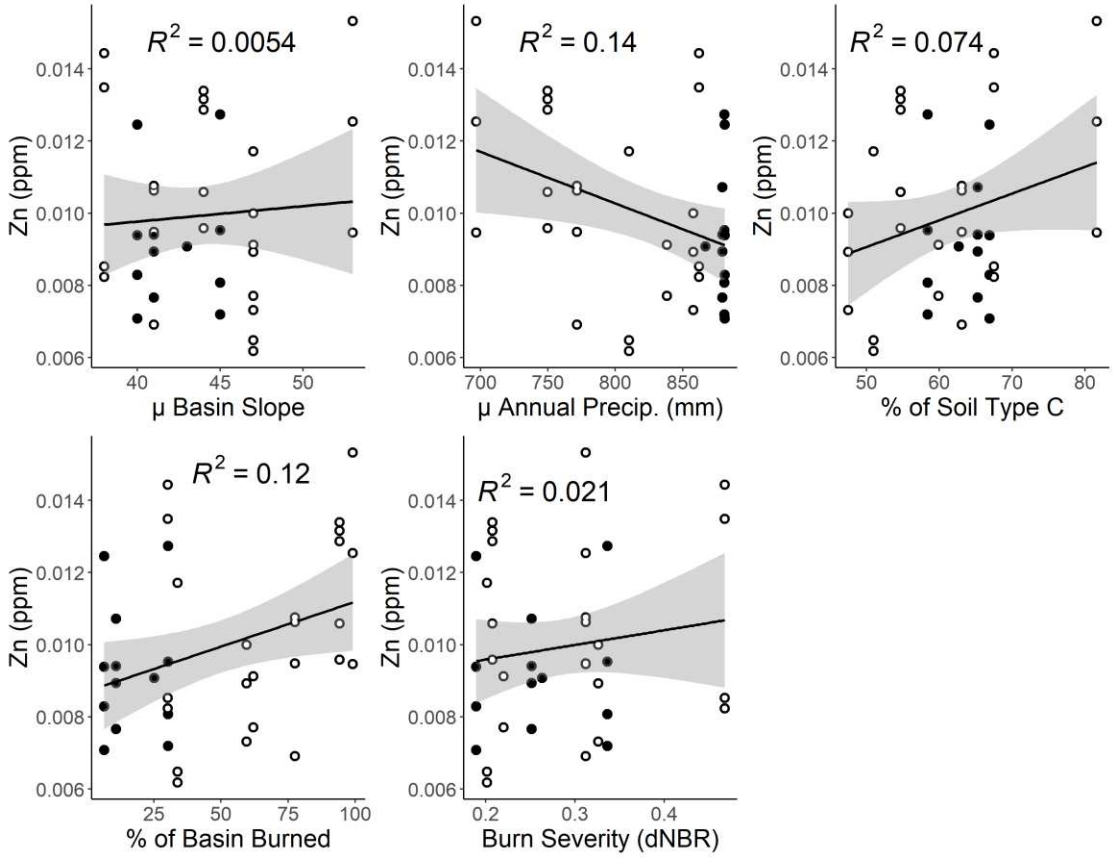

Figure A4: Linear relationships for watershed and burn characteristics for Zn, baseflow filtered (n = 37). Closed dots represent Hermosa drainages and open dots represent tributary drainages. The grey shape shows the standard error with 95% confidence. Coefficient of determination (R^2) is also shown

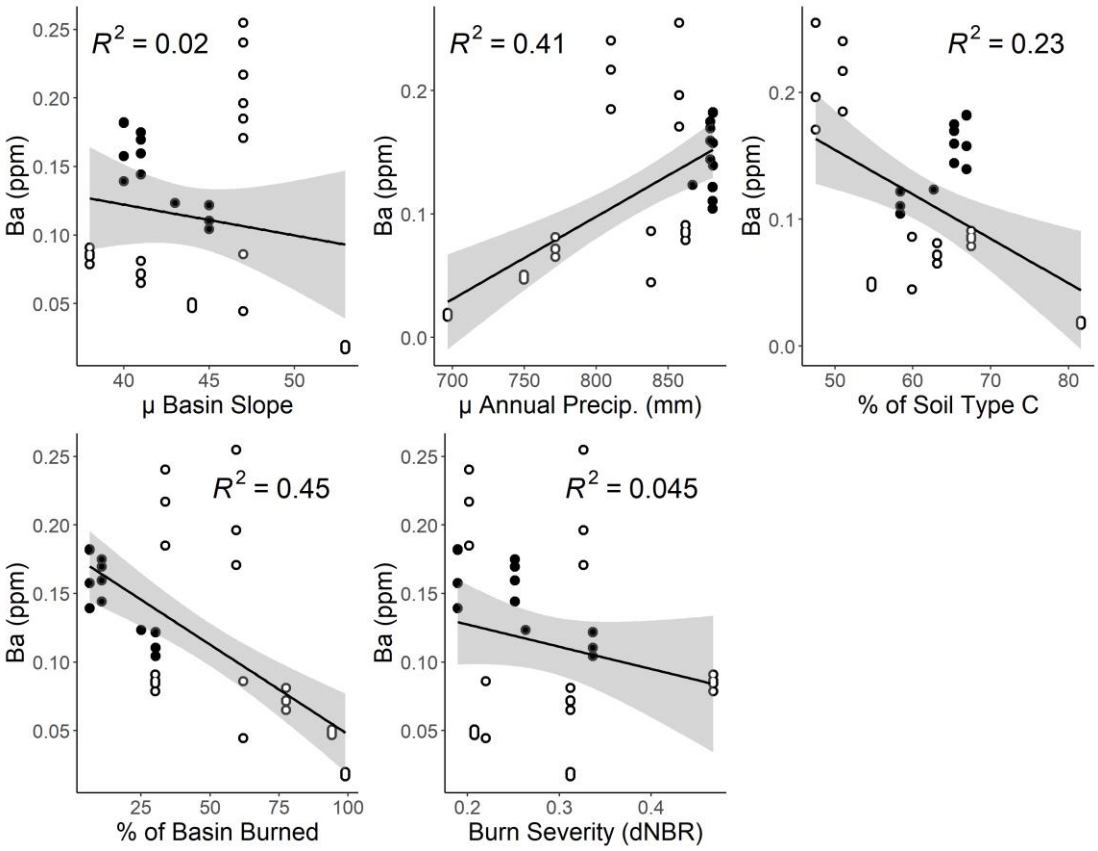

Figure A5: Linear relationships for watershed and burn characteristics for Ba, baseflow filtered (n = 37), Closed dots represent Hermosa drainages and open dots represent tributary drainages. The grey shape shows the standard error with 95% confidence. Coefficient of determination (R^2) is also shown

Table A3: Correlation matrix between all watershed characteristics and burn variables. Correlations are significant where Pearson correlation coefficients are greater than 0.7.

	Basin Slope	Δ Elevation	μ Elevation	Drainage Area	μ Precip.	Soil Type C	Soil Type D	μ dNBR	Max dNBR	% Basin Burned
Basin Slope		0.63	-0.54	-0.17	-0.54	0.00	0.15	-0.21	0.15	0.54
Δ Elevation	0.63		**-0.93**	-0.57	**-0.93**	0.46	-0.16	0.00	0.16	**0.81**
μ Elevation	-0.54	**-0.93**		0.58	**0.95**	-0.27	-0.04	-0.08	-0.19	**-0.94**
Drainage Area	-0.17	-0.57	0.58		0.65	0.03	-0.35	0.04	0.32	-0.62
μ Precip.	-0.54	**-0.93**	**0.95**	0.65		-0.22	-0.09	0.15	0.00	**-0.91**
Soil Type C	0.00	0.46	-0.27	0.03	-0.22		**-0.93**	0.25	0.40	-0.01
Soil Type D	0.15	-0.16	-0.04	-0.35	-0.09	**-0.93**		-0.20	-0.37	0.31
μ dNBR	-0.21	0.00	-0.08	0.04	0.15	0.25	-0.20		0.65	-0.03
Max dNBR	0.15	0.16	-0.19	0.32	0.00	0.40	-0.37	0.65		0.09
% Basin Burned	0.54	0.81	**-0.94**	-0.62	**-0.91**	-0.01	0.31	-0.03	0.09	

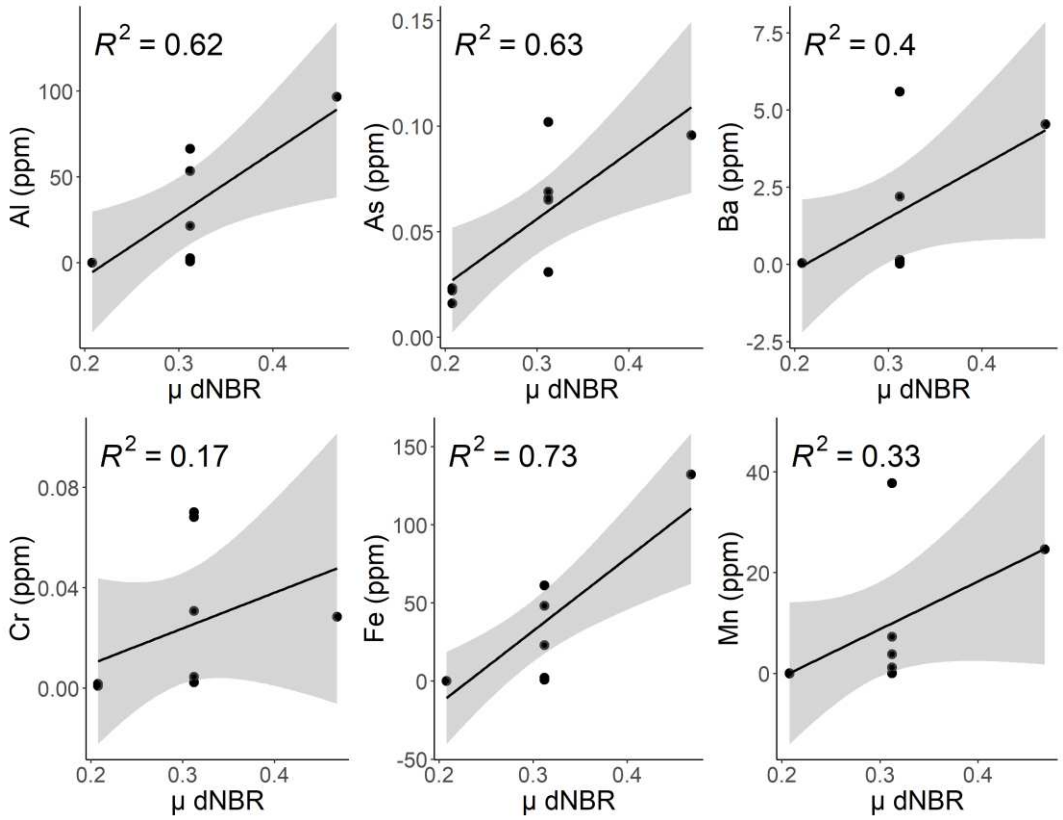

Figure A6: Regression of dNBR for significant pre-storm vs post-storm metals that have concentrations above a drinking water standard.

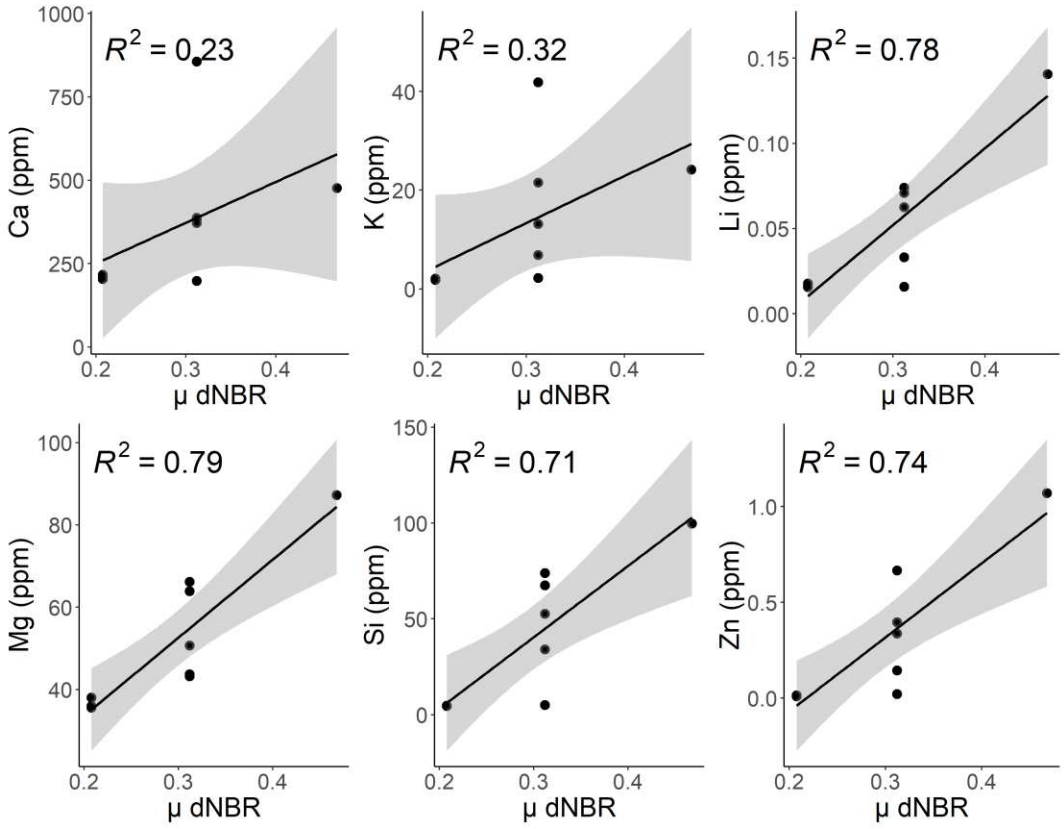

Figure A7: Regression of dNBR for significant pre-storm vs post-storm concentrations